© 2016. Published by The Company of Biologists Ltd | Development (2016) 143, 2946-2957 doi:10.1242/dev.129585

Lizard tail skeletal regeneration combines aspects of fracture healing and blastema-based regeneration

Thomas P. Lozito and Rocky S. Tuan*

ABSTRACT

Lizards are amniotes with the remarkable ability to regenerate amputated tails. The early regenerated lizard tail forms a blastema, and the regenerated skeleton consists of a cartilage tube (CT) surrounding the regenerated spinal cord. The proximal, but not distal, CT undergoes hypertrophy and ossifies. We hypothesized that differences in cell sources and signaling account for divergent cartilage development between proximal and distal CT regions. Exogenous spinal cord implants induced ectopic CT formation in lizard (*Anolis carolinensis*) blastemas. Regenerated spinal cords expressed Shh, and cyclopamine inhibited CT induction. Blastemas containing vertebrae with intact spinal cords formed CTs with proximal hypertrophic regions and distal non-hypertrophic regions, whereas removal of spinal cords resulted in formation of proximal CT areas only. In fate-mapping studies, FITC-labeled vertebra periosteal cells were detected in proximal, but not distal, CT areas. Conversely, FITC-labeled blastema cells were restricted to distal CT regions. Proximal cartilage formation was inhibited by removal of periosteum and could be recapitulated *in vitro* by periosteal cells treated with Ihh and BMP-2. These findings suggest that proximal CTs are directly derived from vertebra periosteal cells in response to BMP and Ihh signaling, whereas distal CTs form from blastema cells in response to Shh signals from regenerated spinal cords.

KEY WORDS: Lizard, Cartilage, Regeneration, Sonic hedgehog, Indian hedgehog, Bone morphogenetic proteins, Growth plate, Ossification, Calcification, Periosteum, Blastema

INTRODUCTION

Lizards are the closest relatives of mammals that exhibit enhanced regenerative abilities of musculoskeletal tissues as adults. As amniotes, lizards follow the same basic blueprints for development, skeletal ossification and wound healing as mammals, yet retain the ability to regenerate amputated tails, a trait shared with urodelian amphibians (Alibardi, 2010). Their distinct evolutionary position intermediate to amphibians and mammals distinguishes lizards from all other regenerative model organisms, and has important and interesting implications in lizard regenerated tissues. Regenerated lizard tails are known as imperfect copies due to several key morphological differences between the regenerated and original tails (Alibardi, 2010; Bellairs and Bryant, 1985; Fisher et al., 2012; Lozito and Tuan, 2015). The most obvious of these differences concerns the regenerated skeleton. Regenerated lizard tail skeletons are almost completely cartilaginous. Vertebrae of the original tail are generated as a single, unsegmented cartilage tube (CT), and the vast majority of the lizard CT resists ossification for the lifetime of the lizard (Lozito and Tuan, 2015). Cartilage is a tissue that most mammals, and humans in particular, have particular difficulty in healing. Lizards, however, represent an organism group that spontaneously generates an abundance of cartilage in response to skeletal injury.

There are generally two mechanisms by which skeletal tissues are regenerated in adult organisms: fracture healing and blastema-based regeneration. In fracture healing, periosteal stem cells activated by the wound environment proliferate and differentiate into cartilage, forming a cartilage callus that bridges the gap between broken bones (Roberts et al., 2015). Callus cartilage development follows many of the same stages as embryonic endochondral ossification and is regulated by a conserved set of pathways. For example, periosteal stem cells proliferate in response to bone morphogenetic protein (BMP) signaling (Wang et al., 2011), and callus chondrocytes regulated by Indian hedgehog (Ihh) signaling undergo hypertrophy and express markers such as alkaline phosphatase (Alk Phos) (Wang et al., 2010). Eventually the cartilage callus ossifies and reforms a periosteum, leading to complete fracture healing.

Regrowth of amputated skeletal elements involves blastema-based regeneration. The term ‘blastema’ refers to a mass of cells that act as progenitors for regenerated tissues. The capacity to form blastemas decreases dramatically with age, and lizards are the only amniotes capable of blastema-based regeneration as adults. Unlike the urodeles, lizards are unable to regenerate amputated limbs, distinguishing lizards as the only adult organisms to combine regenerative (tail) and non-regenerative (limbs) appendages in the same animal (Alibardi, 2010). We have previously characterized development of the regenerated lizard tail skeleton, the CT, which involves blastema-based healing (Lozito and Tuan, 2015). Immediately after tail loss, the tail stump ends in a terminal tail vertebra and involves a severed spinal cord. After 7-10 days, wound epidermis migrates over the tail stump and thickens to form an apical cap. Cells liberated from stump tissues collect under the apical cap and proliferate to form a blastema. The spinal cord regenerates and infiltrates the blastema. The regenerated lizard tail spinal cord is characterized by a prominent ependymal tube. After another week, the CT forms around the regenerated spinal cord and makes contact with the terminal tail vertebra at its proximal end.

We have observed important differences in development and behavior between proximal and distal regions of regenerated lizard tail skeletons (Lozito and Tuan, 2015). Extreme proximal cartilage regions in contact with the original tail vertebrae resemble cartilage calluses formed during mammalian fracture repair. These proximal cartilage regions also exhibit growth plate-like properties and undergo a process similar to endochondral ossification. For example, proximal cartilage chondrocytes undergo hypertrophy, as evidenced by increases in cell size and expression of the

Center for Cellular and Molecular Engineering, Department of Orthopaedic Surgery, University of Pittsburgh School of Medicine, Pittsburgh, PA 15219, USA.

*Author for correspondence (rst13@pitt.edu)

T.P.L., 0000-0002-6855-3571

Received 7 August 2015; Accepted 14 June 2016

Development (2016) 143, 2946-2957 doi:10.1242/dev.129585

hypertrophic chondrocyte markers BMP-6 and Alk Phos. Ossification centers form in between terminal tail vertebrae and proximal cartilage, setting up growth plate-like zones in these regions, which eventually undergo endochondral ossification and are replaced by bone that is continuous with that of original tail vertebrae. This endochondral ossification process is limited to proximal callus-like areas, and does not proceed to distal CT regions. The perichondria of distal CTs calcify, but never develop the growth plate-like structures observed in proximal areas, and distal CTs resist transitioning to bone for the lifetime of the lizards.

This study aims to determine the reasons why proximal, but not distal, regenerated lizard tail skeletons undergo hypertrophy and endochondral ossification. We hypothesize that differences in signaling and cell sources account for divergent development between the proximal and distal regenerated cartilage. Although the topics of cell source and signaling have been addressed in regenerated tissues of other model organisms with modern techniques (Kragl et al., 2009; Rinkevich et al., 2011; Sandoval-Guzman et al., 2014; Stewart and Stankunas, 2012), they have only recently received similar attention in lizards (Bai et al., 2015; Hutchins et al., 2014; Lozito and Tuan, 2015). Furthermore, studies considering regenerated lizard tails performed in the 1960s have remained largely unchallenged and yet are at odds with more recent reports on salamander limb and tail regeneration, particularly relating to cell sources (Cox, 1969; Kragl et al., 2009; Sandoval-Guzman et al., 2014). Here, we distinguish between cells and signals derived directly from the tissues of the original lizard tail versus those derived from the blastema to determine their specific contributions to the regenerated lizard tail skeleton. We conclude that proximal cartilage regions are derived directly from the periosteum of the original tail vertebrae, whereas distal CTs form from blastemal cells in response to signals from the regenerated spinal cord. In fact, our results suggest that proximal cartilage regions of regenerated lizard tail skeletons form independently of blastema-derived, distally located 'true' CTs. In recognition of these distinctions and to avoid confusion, hereafter we refer to the proximal regenerated lizard tail skeleton as the cartilage callus (CC) (equivalent to the 'proximal CT' term used in the Abstract and in previous publications; Lozito and Tuan, 2015). Similarly, the term CT will be used to describe all regions of regenerated lizard tail skeletons except the proximal CC that eventually ossifies (equivalent to the 'distal CT' term used in the Abstract and in previous publications; Lozito and Tuan, 2015). Finally, anterior, medial and posterior are used to designate specific regions within CC and CT regions (i.e. medial CC, anterior CT, etc.).

RESULTS

Regenerated lizard spinal cord implants induce ectopic CTs

The regenerated spinal cord and ependymal tube have previously been shown to induce cartilage formation in regenerated salamander tails (Holtzer, 1956; Schnapp et al., 2005), and here we tested whether regenerated spinal cords play similar roles in lizard tail regeneration. Spinal cords were isolated from donor regenerated lizard tails (see Fig. S2 for spinal cord isolation procedure), and pieces were implanted into distal regions of recipient blastemas to create tails with both endogenous and exogenous spinal cords, which were analyzed for cartilage development after 14 days (Fig. 1A) (see Fig. S3 for spinal cord implantation procedure). Control tails that did not receive any regenerated spinal cord implants developed single cartilage tubes around endogenous regenerated spinal cords (5/5 tails examined) (Fig. 1B). Experimental tails that received exogenous spinal cord implants formed multiple cartilage tubes (21/24) (Fig. 1C), including single endogenous cartilage tubes around endogenous spinal cords (Fig. 1D) and ectopic cartilage tubes surrounding regenerated spinal cord implants (Fig. 1E-G). Both endogenous regenerated spinal cords (Fig. 1H,I) and exogenous spinal cord implants (Fig. 1J-L) exhibited prominent ependymal tubes that expressed the ependymal cell marker glial fibrillary acidic protein (GFAP) (Fig. 1H-L). Regenerated spinal cord ependymal cells also expressed high levels of the morphogen sonic hedgehog (Shh) (Fig. 1M-Q). These results suggested that lizard CTs are induced by regenerated spinal cords.

Hedgehog regulates lizard CT induction

Shh produced by ependymal tubes of regenerated spinal cords was previously shown to be responsible for induction of cartilage skeletons in regenerated salamander tails (Schnapp et al., 2005) and the following set of experiments sought to determine whether Shh plays a similar role in regenerated lizard tail skeletal development. As described above, the ependymal tubes of regenerated lizard tails express high levels of Shh (Fig. 1M-Q), and here we directly tested the role of hedgehog in lizard CT induction. Beads soaked in the hedgehog inhibitor cyclopamine, the hedgehog agonist SAG, and/or vehicle controls were grafted to the dorsal and/or ventral surfaces of distal blastema explants. Explants grafted with vehicle control beads developed typical CTs that completely encircled ependymal tubes (10/10 explants examined) (Fig. 2A). Grafting of cyclopamine beads to the dorsal surfaces of explants restricted cartilage formation to ventral blastema regions (10/10) (Fig. 2B), whereas explants with cyclopamine beads grafted to ventral surfaces formed cartilage that was restricted to dorsal regions (10/10) (Fig. 2C). Cartilage formation was completely inhibited in blastemas that received both dorsal and ventral cyclopamine beads (8/10) (Fig. 2D). Cyclopamine-induced loss of cartilage could be rescued by simultaneously grafting SAG and cyclopamine beads into dorsal blastemas (7/10) (Fig. 2E). In summary, cyclopamine inhibited chondrogenesis in surrounding areas and restricted cartilage formation to opposite sides of ependymal tubes, which expressed high levels of Shh. Taken together, these results suggested that the lizard CT forms from blastema cells in response to Shh signals from the ependymal tube of the regenerated spinal cord.

The effects of Shh and other growth factors with known effects on mammalian chondrogenesis were also directly tested on lizard tail blastema cells *in vitro*. Cells isolated from blastemas were pellet cultured and treated with 10 ng/ml Shh, TGF-β1, BMP-2 or FGF-2 for 21 days (Fig. 2F-K). Only Shh-treated pellets developed significant cartilage areas, which were located along the periphery of the blastema cell pellets (Fig. 2G). These results supported the specificity of hedgehog signaling in inducing blastema cell chondrogenesis.

Proximal regenerated lizard tail skeletons are induced by vertebrae, whereas distal regions are induced by ependymal tubes

We next examined the effects of ependymal tube removal with experiments testing the individual activities of vertebrae and ependymal tubes in proximal and distal cartilage formation. Two groups of blastema explants (Fig. 3A), one with vertebrae and ependymal tubes intact, and one in which ependymal tubes were removed (see Fig. S4 for ependymal tube removal procedure), were assayed for cartilage development. Tails with both vertebrae and ependymal tubes developed skeletons with both proximal CCs and distal CTs (5/5 tails examined) (Fig. 3B), whereas tails containing

Development (2016) 143, 2946-2957 doi:10.1242/dev.129585

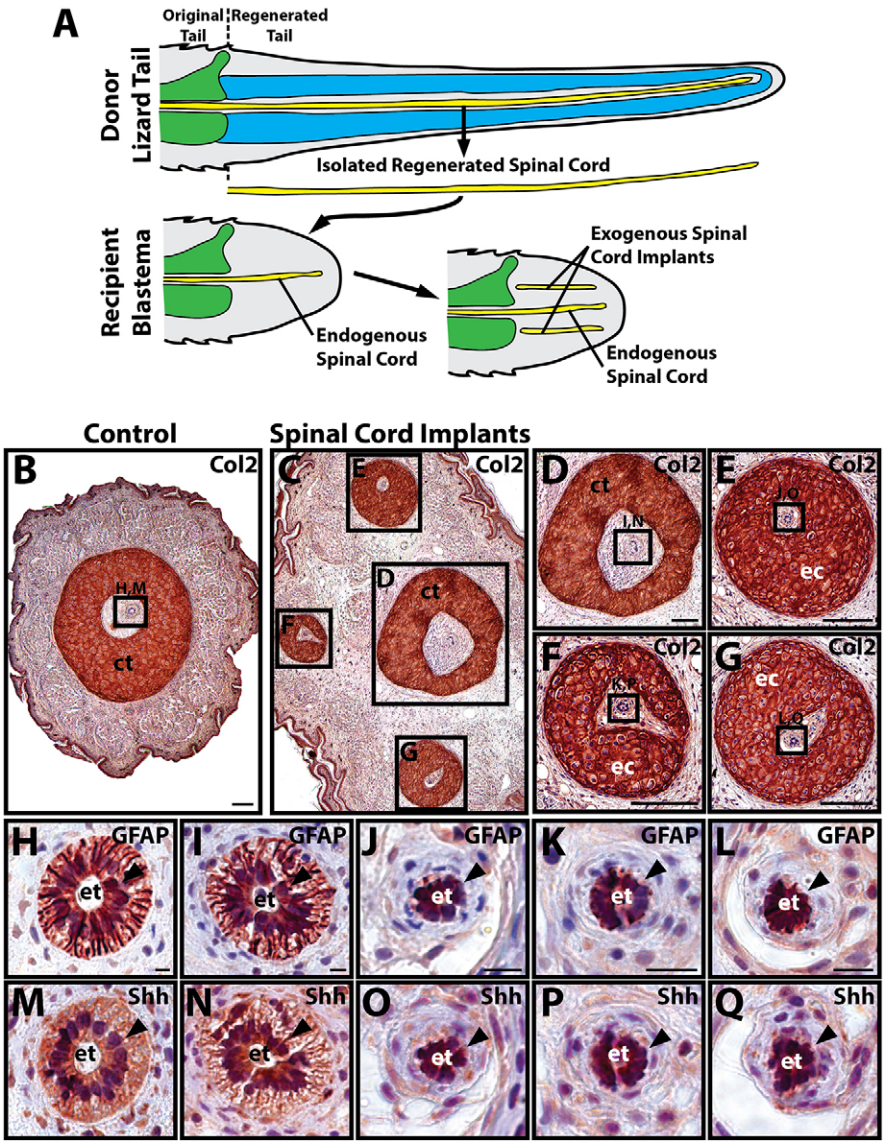

Fig. 1. Lizard regenerated spinal cord implants induce ectopic cartilage formation. (A) Schematic showing experimental set-up for spinal cord implantation studies. Regenerated spinal cords were isolated from donor regenerated lizard tails and implanted into recipient lizard blastemas. Control blastemas contained endogenous spinal cords, whereas experimental blastemas contained both endogenous spinal cords and exogenous spinal cord implants. (B-G) Control blastemas (B) and experimental blastemas with spinal cord implants (C-G) were analyzed by Col2 IHC. Control blastemas (B) formed endogenous CTs around endogenous spinal cords, whereas experimental blastemas formed endogenous CTs around endogenous spinal cords (D) and ectopic CTs around spinal cord implants (E-G). (H-Q) Higher magnification views of endogenous and exogenous regenerated spinal cord regions identified in B,D-G. Endogenous spinal cords (H,I,M,N) and exogenous spinal cord implants (J-L,O-Q) exhibited prominent ependymal tubes (black arrowheads) that expressed GFAP (H-L) and Shh (M-Q). ct, cartilage tube; ec, ectopic cartilage tube; et, ependymal tube. Scale bars: 100 µm (B-G); 12.5 µm (H-Q).

vertebrae without ependymal tubes developed proximal CC areas only (5/5) (Fig. 3C). CTs did not form in samples in which regenerated spinal cord tissue other than ependymal tube remained following surgical manipulations, validating the dependency of CT formation on intact ependymal tubes. In skeletons with both CC and CT regions, proximal CCs underwent hypertrophy and expressed Alk Phos (5/5) (Fig. 3D), whereas distal CTs did not undergo hypertrophy or express Alk Phos (5/5) (Fig. 3E). Proximal CCs formed after spinal cord removal also exhibited hypertrophic morphologies and Alk Phos expression (5/5) (Fig. 3F). These results reinforced the conclusion that lizard CTs are induced by signals originating from the regenerated spinal cord ependymal tube, and introduced the idea that proximal CCs are induced and influenced by signals from the vertebra.

Proximal regenerated lizard tail cartilage hypertrophy is regulated by signals originating from original tail vertebrae

Numerous lines of evidence supported the link between CC hypertrophy and original tail vertebrae. Results from spinal cord implant studies indicated that, in the absence of vertebrae, proximal cartilage did not undergo hypertrophy (Fig. S8). Pro-hypertrophy effects were specific for vertebral tissue. Lizard tails re-amputated in regenerated CT portions did not develop hypertrophic cartilage regions (Fig. S9). Similarly, non-vertebral original tail stump tissues did not induce hypertrophy in CCs (Fig. S10). Finally, we performed experiments specifying lizard tail vertebrae, and the periosteum in particular, as sources of pro-hypertrophy signals (Fig. S11). Indeed, lizard periosteal cells induce hypertrophic markers in CC, but not CT, cells (Fig. S12). Taken together, these results demonstrated that signals responsible for inducing hypertrophy in proximal regenerated lizard tail cartilage originate from original tail vertebrae, and the following group of studies aimed to identify the specific signals involved.

Hedgehog signaling regulates proximal cartilage induction and hypertrophy

Western blot analysis of growth factors expressed by the proximal CC identified Ihh, BMP-2 and BMP-6 as the most abundant/detectable (Fig. S13) and spatially distinct (Fig. S14). The next set of experiments investigated the specific roles of each of these molecules in proximal cartilage development. The first group of experiments focused on hedgehog signaling via Ihh. Ihh expression begins around 12 days post-amputation (DPA) and increases in the CC over the first 21 days of regenerated lizard tail cartilage

Development (2016) 143, 2946-2957 doi:10.1242/dev.129585

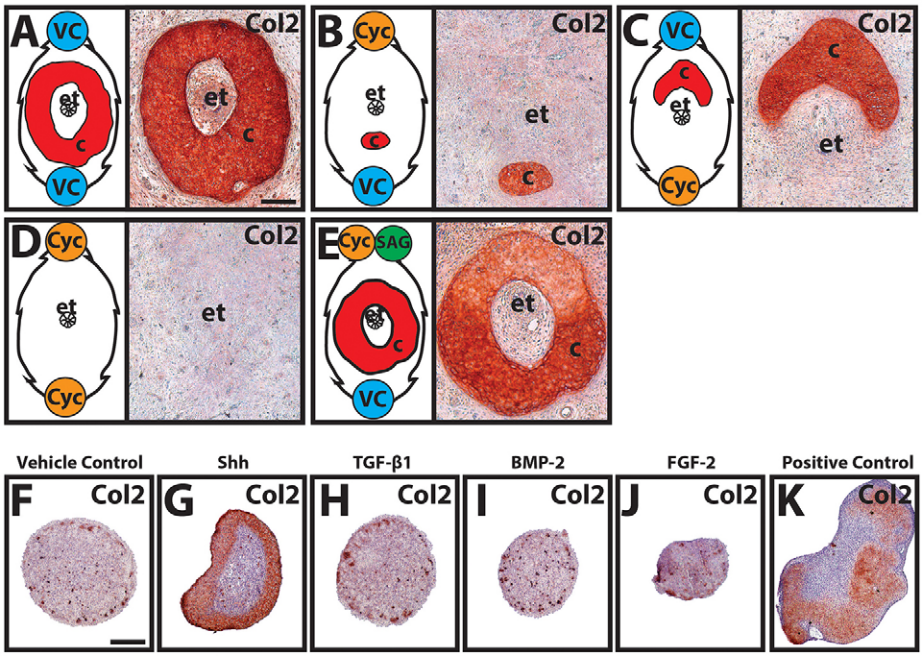

Fig. 2. Manipulation of lizard CT patterning with cyclopamine and SAG. (A-E) Beads soaked in cyclopamine (Cyc), SAG, and/or vehicle control (VC) were grafted to the dorsal (top) and/or ventral (bottom) surfaces of lizard blastemas, explant-cultured for 14 days, and analyzed by Col2 IHC. Line drawings on the left of each panel illustrate relative positions of implanted beads and effects on cartilage formation. Cyclopamine beads inhibited cartilage formation in neighboring areas, and cartilage induction was rescued by co-treatment with SAG. (F-J) Lizard blastema cells pellet-cultured and treated with 10 ng/ml Shh, TGF-β1, BMP-2, FGF-2 or vehicle control for 21 days were immunostained for Col2. (K) Lizard embryonic limb bud cell pellets served as positive controls for chondrogenesis. c, cartilage; et, ependymal tube. Scale bars: 100 µm.

formation (Fig. S15). During this time-frame, Ihh expression is restricted to the proximal CC rather than the distal CT (Fig. S15). To test the role of Ihh and hedgehog signaling in early CC formation, nine DPA blastema explants were treated with vehicle control or cyclopamine for 7 days, during the inductive phase of proximal cartilage tube development. Whereas vehicle control samples developed proximal CCs of normal appearance (7/7 explants examined) (Fig. 4A), treatment with cyclopamine inhibited proximal cartilage formation (9/9) (Fig. 4B). Cyclopamine-induced loss of cartilage formation could be rescued by co-treatment with SAG (7/9) (Fig. 4C). To validate the hypothesis that cyclopamine and SAG were acting through hedgehog inhibition rather than modulation of hedgehog expression, the same samples were analyzed by Ihh immunostaining (Fig. 4D-F). Neither cyclopamine nor SAG treatment significantly affected Ihh expression levels, suggesting that the observed effects on cartilage formation were, in fact, signaling effects of drug treatments. Thus, these results suggested that proximal cartilage formation is induced by Ihh signaling.

The next set of experiments involved treating blastema explants with cyclopamine beginning after CC formation (14 DPA) to focus on the role of hedgehog in later stages of cartilage development. Proximal CCs of explants treated with vehicle control underwent hypertrophy (9/9 explants examined) (Fig. 5A), as indicated by cell morphology (Fig. 5A,D) and Alk Phos expression (Fig. 5D), whereas cyclopamine treatment inhibited hypertrophy (9/9) (Fig. 5B,E) and Alk Phos expression (9/9) (Fig. 5E). Co-treatment with SAG partially rescued cartilage hypertrophic

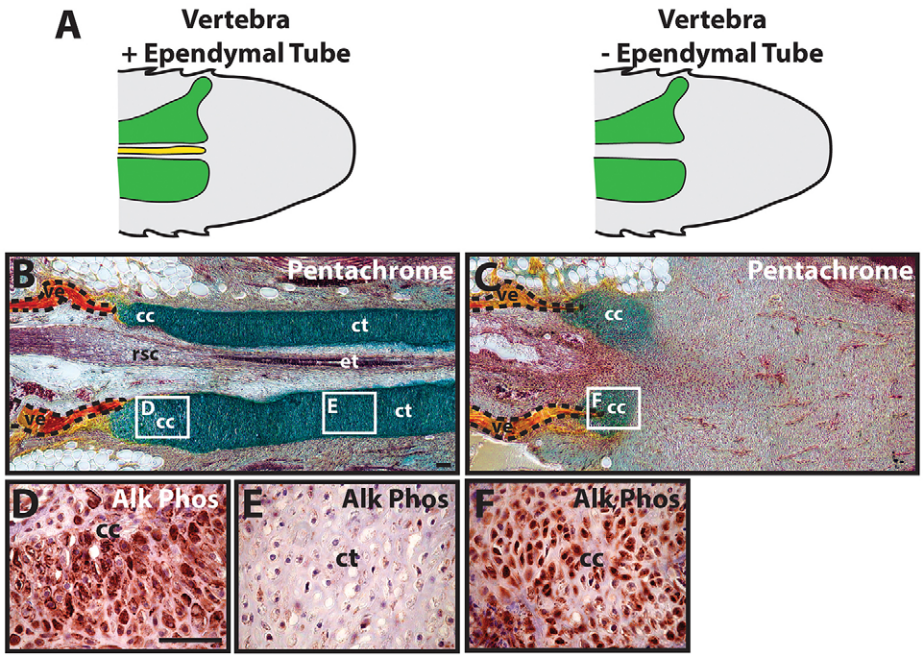

Fig. 3. Proximal and distal regenerated lizard tail skeletal regions form independently. (A) Lizard tail blastemas, with or without endogenous ependymal tubes, were studied for differences in cartilage development. (B,C) The effects of ependymal tube removal on cartilage formation was analyzed by pentachrome staining. Tails with both vertebrae and ependymal tubes developed both proximal CCs and distal CTs (B), whereas tails lacking ependymal tubes developed CC areas only (C). (D-F) Higher magnification views of CC (D,F) and CT (E) areas analyzed by Alk Phos IHC. Vertebrae boundaries are traced in dashed lines. cc, cartilage callus; ct, cartilage tube; et, ependymal tube; rsc, regenerated spinal cord; ve, vertebra. Scale bar: 100 µm.

Development (2016) 143, 2946-2957 doi:10.1242/dev.129585

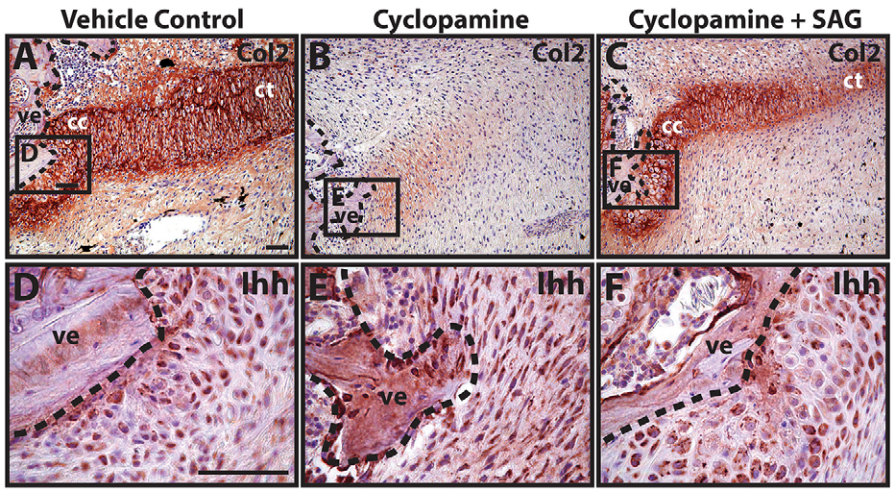

Fig. 4. Cyclopamine inhibits proximal cartilage induction. (A-C) Lizard tail blastema explants (9 DPA) were treated with vehicle control (A), cyclopamine (B) or cyclopamine and SAG (C) and analyzed by Col2 immunostaining to assess the role of hedgehog signaling in proximal CC formation. (D-F) Higher magnification views of regions identified in A-C analyzed by Ihh immunostaining. Dashed lines trace vertebral boundaries. cc, cartilage callus; ct, cartilage tube; ve, vertebra. Scale bars: 50 µm.

morphology (8/9) (Fig. 5C,F) and Alk Phos expression (7/9) (Fig. 5F), although the hypertrophic regions appeared disorganized (Fig. 5C) compared with controls. Samples were also analyzed by BMP-6 immunostaining (Fig. 5G-I) to gain a better understanding of the interplay between hedgehog and BMP signaling. Hypertrophic chondrocyte regions expressed BMP-6 under control conditions (Fig. 5G). Cyclopamine treatment significantly inhibited BMP-6 expression in these regions (9/9) (Fig. 5H), and co-treatment with SAG partially rescued BMP-6 expression levels (9/9) (Fig. 5I). Alk Phos and BMP-6 immunostaining results were validated by western blotting (Fig. 5J,K). Taken together, these results suggested that hedgehog signaling regulated proximal CC hypertrophy and acted to induce BMP-6 expression in hypertrophic cartilage regions.

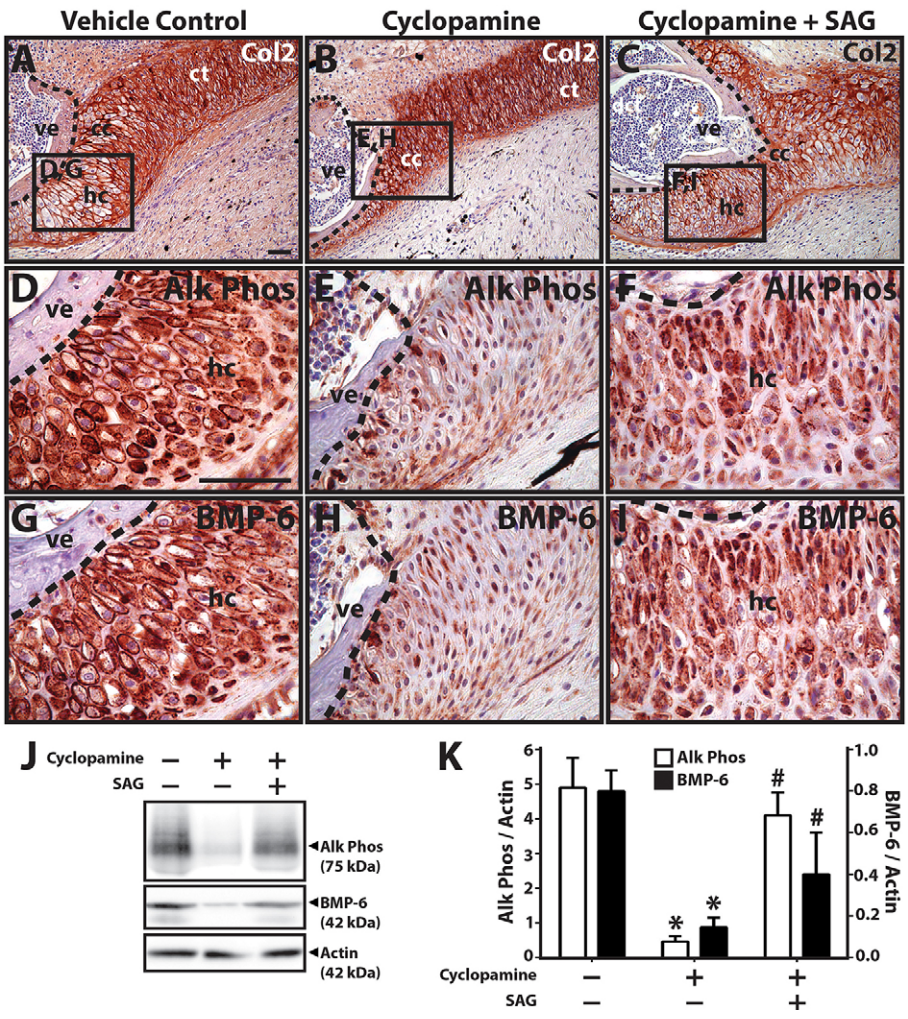

Fig. 5. Cyclopamine inhibits proximal cartilage hypertrophy. (A-C) Lizard tail blastema explants (14 DPA) were treated with vehicle control (A), cyclopamine (B) or cyclopamine and SAG (C) and analyzed by Col2 immunostaining to assess the role of hedgehog signaling in proximal CT hypertrophy. (D-I) Higher magnification views of regions identified in A-C analyzed by Alk Phos (D-F) and BMP-6 (G-I) expression. Dashed lines trace vertebral boundaries. (J) Western blot analysis of Alk Phos and BMP-6 expression in CC explants treated with vehicle control, cyclopamine and/or SAG. Actin blots were included as loading controls. (K) Densitometric quantification of Alk Phos and BMP-6 western blot results normalized to actin loading controls (n=3). *P<0.05 compared with vehicle controls; $^{\#}P$<0.05 compared with 0 ng/ml SAG condition; Student's t-test. Data are mean±s.d. cc, cartilage callus; ct, cartilage tube; hc, hypertrophic chondrocytes; ve, vertebra. Scale bars: 50 µm.

Development (2016) 143, 2946-2957 doi:10.1242/dev.129585

Interestingly, treatment with Ihh-soaked beads did not significantly induce exogenous regions of proximal or distal cartilage (Fig. S16). Similarly, none of the SAG treatments described above induced cartilage in blastema areas that would otherwise form other tissues, such as muscle. These results suggest that cartilage formation within the regenerated lizard tail is not only dependent upon hedgehog signaling, but is also influenced by the responsiveness of the cell population, an idea that is further explored in the experiments concerning cartilage cell origins described below.

BMP signaling regulates proximal cartilage proliferation and hypertrophy

The final set of drug/growth treatment experiments tested the effects of BMP inhibition and stimulation on proximal CC development. Explants (9 DPA) treated with vehicle control exhibited normal, fully developed CCs (9/9 explants examined) (Fig. 6A). Treatment with the BMP antagonist noggin resulted in gaps between CCs and distal CTs (8/9) (Fig. 6B), and treatment with exogenous BMP-2 caused significant enlargement of proximal CCs (9/9) (Fig. 6C). These results suggested an effect on proliferation, so we assayed for proliferation with bromodeoxyuridine (BrdU) immunostaining (Fig. 6D-F). Inhibition of BMP signaling by treatment with noggin resulted in a reduction of proliferative cells in proximal CC areas (9/9) (Fig. 6E), suggesting that BMP regulated proliferation of this region. BrdU-positive proliferating chondrocytes were smaller than non-proliferating cells (Fig. 6D,F), and proximal CCs of noggin-treated samples were almost entirely made up of larger, rather than smaller, cells (Fig. 6E). The reduced numbers of these smaller, proliferating chondrocytes in non-union areas of noggin-treated samples suggested that noggin treatment caused reductions in proliferating chondrocyte populations.

We also noticed differences in hypertrophic region sizes among the three conditions (Fig. 6A-C), and staining for Alk Phos expression (Fig. 6G-I) confirmed that noggin treatment inhibited hypertrophy (9/9) (Fig. 6H) and BMP-2 treatment enhanced hypertrophy (9/9) (Fig. 6I) compared with vehicle controls (Fig. 6G). These results suggested that BMP signaling also regulated proximal CC hypertrophy. The same samples were also analyzed for BMP-6 (Fig. 6J-L) and Ihh (Fig. 6M-O) expression. Noggin treatment decreased BMP-6 expression levels (9/9) (Fig. 6K), and BMP-2 treatment enhanced BMP-6 expression (9/9) (Fig. 6L). Neither noggin (Fig. 6N) nor BMP-2 (Fig. 6O) treatment significantly affected Ihh expression levels, although noggin treatment resulted in disorganized Ihh expression less closely associated with vertebrae (Fig. 6N) compared with control and BMP-2 conditions (Fig. 6M,O). Observations on the effects of noggin and BMP-2 on CC cell proliferation were quantified with cell proliferation assays (Fig. 6P), and Alk Phos and BMP-6 immunostaining results were verified by western blots (Fig. 6Q,R). Taken together, these results suggested that BMP signaling regulates both primal CC proliferation and hypertrophy. Furthermore, as hedgehog inhibition reduced BMP expression, and BMP inhibition reduced BMP but not Ihh expression, these results support the hypothesis that BMP regulates its own expression and acts downstream of Ihh in proximal CC development.

Proximal regenerated lizard tail skeletons are directly derived from vertebrae periosteum, whereas more distal regions are derived from blastema cells

Having shown that the proximal and distal regenerated lizard tail skeletal regions were regulated by signals originating from different tissues, we wanted to determine whether the cell sources of the two regions also differed. These experiments were also motivated by

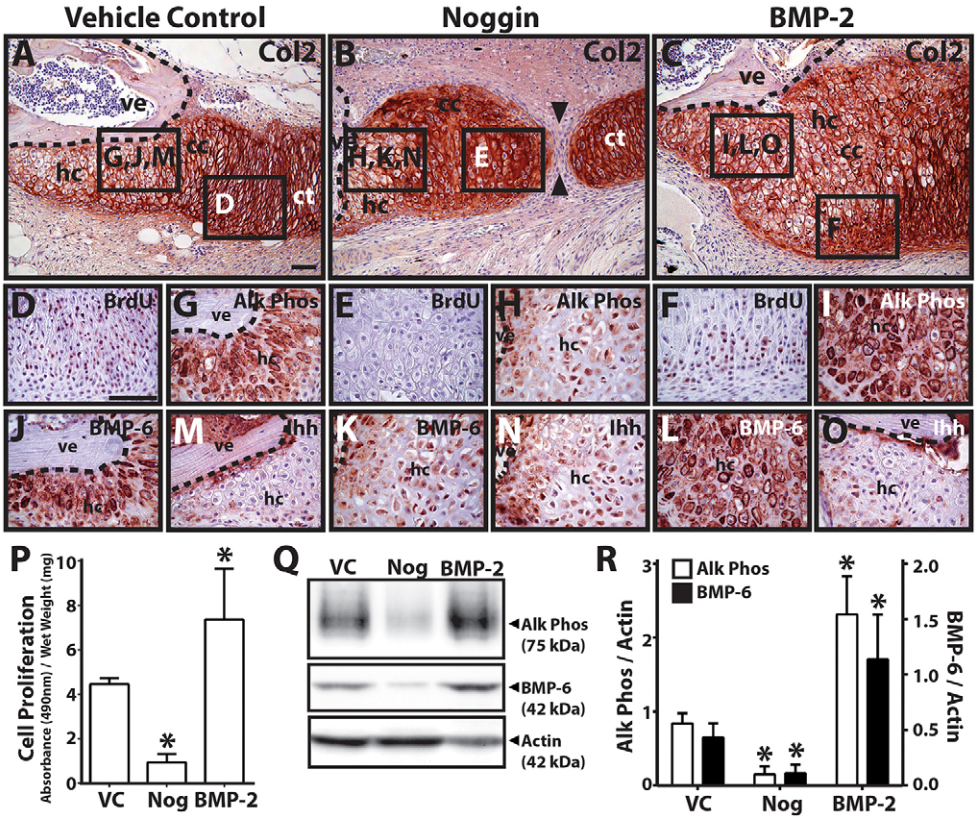

Fig. 6. BMP inhibition and stimulation modulates proximal cartilage proliferation and hypertrophy. (A-C) Lizard tail blastema explants (9 DPA) were treated with vehicle control (A), noggin (B) or BMP-2 (C) and analyzed by Col2 immunostaining to assess the role of hedgehog signaling in proximal CT hypertrophy. Noggin treatment resulted in non-unions between proximal and distal CT regions (black arrowheads). (D-O) Higher magnification views of regions identified in A-C analyzed by BrdU (proliferating cells; D-F), Alk Phos (G-I), BMP-6 (J-L) and (M-O) Ihh immunostaining. Dashed lines trace vertebral boundaries. (P) Quantification of cell proliferation in CC explants treated with vehicle control (VC), noggin (Nog) or BMP-2 (n=3). *P<0.05 compared with vehicle control; Student's t-test. (Q) Western blot analysis of Alk Phos and BMP-6 expression in CC explants treated with VC, noggin or BMP-2. Actin blots were included as loading controls. (R) Densitometric quantification of Alk Phos and BMP-6 western blot results normalized to actin loading controls (n=3). *P<0.05 compared with vehicle controls; Student's t-test. Data are mean±s.d. cc, cartilage callus; ct, cartilage tube; hc, hypertrophic chondrocytes; ve, vertebra. Scale bars: 50 µm.

Development (2016) 143, 2946-2957 doi:10.1242/dev.129585

considering wound healing in lizard skeletal tissues outside of the tail. Although lizards can regenerate amputated tails, they are unable to regrow lost limbs, so limb and tail injuries were compared to identify healing responses common to both tissues and, thus, independent of blastema-based regeneration. Amputated lizard limbs and toes do not form blastemas (0/10 limbs/toes examined), but significant CCs do form around the damaged bone (10/10) (Fig. S17A) that express Col2 (10/10) (Fig. S17B) and Alk Phos (10/10) (Fig. S17C), similar to the proximal CCs of regenerated tail skeletons. These observations suggested the possibility that proximal cartilage originates from the bones of original tails and forms independently of blastema-derived regenerated cartilage.

To test this hypothesis directly, vertebral cell fate-mapping experiments were performed. Lizard tail vertebral tissue was treated with carboxyfluorescein diacetate-succinimidyl ester (CFDA-SE), which irreversibly labels cells with FITC, and implanted into unlabeled blastema explants (Fig. 7A). After 2 weeks of culture, explants were assayed for co-expression of FITC, Col2 and Alk Phos to identify Alk Phos^{+} cartilage regions directly derived from vertebral tissue (Fig. 7B). A significant majority of FITC-positive cells were detected in proximal Alk Phos^{+} CCs rather than distal Alk Phos^{-} CTs (n=5 explants) (Fig. 7C-F), suggesting that proximal cartilage is directly derived from vertebrae. Penetration of the labeling reagent was found to be restricted to the periosteum of CDFA-treated vertebral tissue (Fig. S18A,B), suggesting that the periosteum is the specific tissue source of the proximal CC. Lizard tail vertebra periosteum could be efficiently removed (Fig. S18C,D), and periosteal cells were isolated from periosteal tissue and cultured *in vitro* (Fig. S18E). Isolated periosteal cells expressed the stem/progenitor cell markers CD166, CD144 and CD90 (Fig. S19). Interestingly, isolated CC, but not CT, cells also expressed these markers, strengthening the finding that the lizard tail CC is derived from periosteal cells (Fig. S19A). Periosteal cells alone expressed high levels of Ihh (Fig. S19A,E), indicating these cells, rather than CC cells, as the original source for Ihh in the regenerating lizard tail. Having also shown that lizard periosteal cells induce Ihh in CC cells during co-culture (Fig. S12), these results also suggest that CC Ihh is induced by periosteal cells. Finally, we tested the dependency of CC formation on vertebra periosteum (Fig. S20), finding that removal of periostium resulted in loss of CC formation (Fig. S20B,C), and that isolated periosteal cells formed cartilage *in vitro* (Fig. S20D-F). Furthermore, periosteal cells proliferated and migrated in response to BMP stimulation (Fig. S21). Taken together, these results suggested that proximal CCs are derived from periosteal cells.

To validate these results, the reverse experiment, in which unlabeled vertebrae were implanted into FITC-labeled blastemas (Fig. 7G), was also performed. The same type of analysis as described above was conducted, but here regions that expressed both FITC and Col2 represented cartilage derived from blastema cells (Fig. 7H). In these experiments, FITC was only detected in Alk Phos^{-} CT areas,

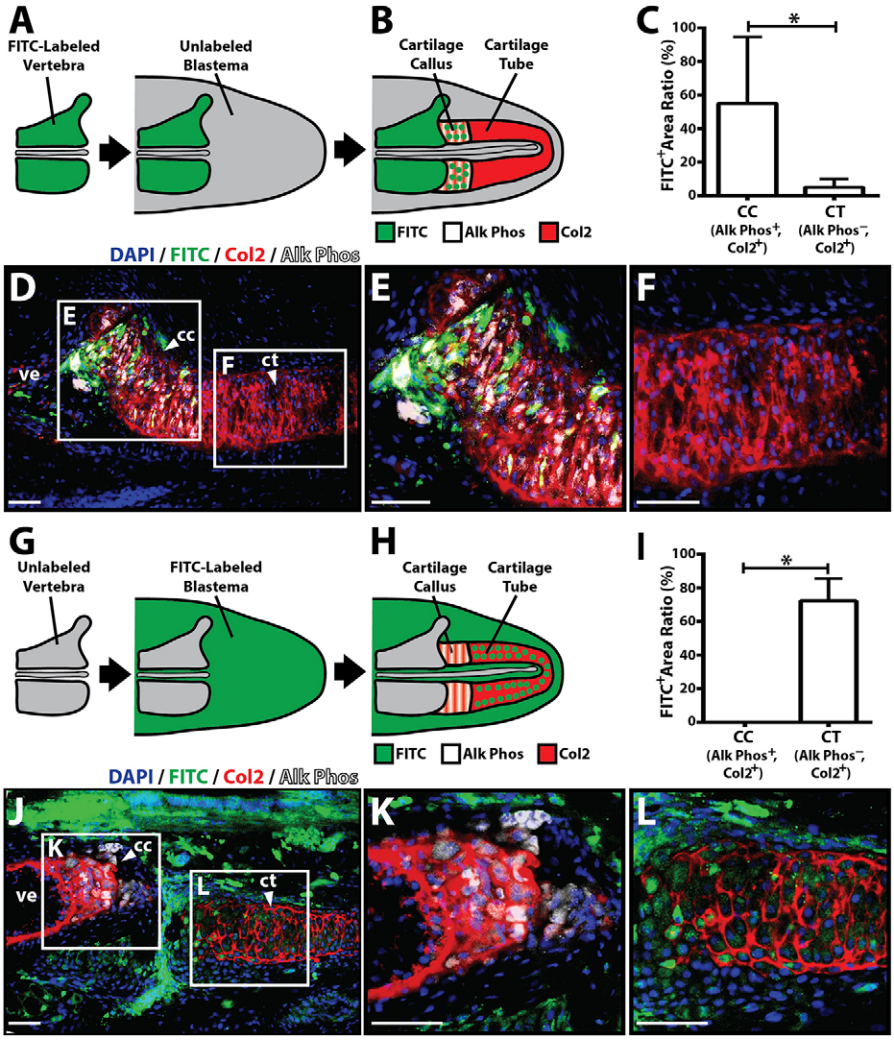

Fig. 7. Vertebral and blastema cells fate map to proximal and distal regenerate lizard tail skeletal regions, respectively. (A,B) Experimental scheme used to fate map vertebral-derived cartilage regions. (A) FITC-labeled vertebrae were implanted into unlabeled blastema explants. (B) After 2 weeks, during which time CCs/CTs formed, samples were co-immunostained for Alk Phos and Col2 to determine whether FITC-labeled cells traced to Alk Phos^{+} Col2^{+} cartilage callus (CC) regions or Alk Phos^{-} Col2^{+} cartilage tube (CT) regions. (C) Areas of FITC^{+}, Alk Phos^{+} and Col2^{+} regions were quantified using ImageJ and compared between Alk Phos^{+} Col2^{+} CC regions and Alk Phos^{-} Col2^{+} CT regions (n=5). *P<0.05; Student's t-test. (D) Representative unlabeled blastema sample implanted with FITC-labeled vertebra following 2 weeks of explant culture and analyzed for FITC, Col2 and Alk Phos expression. (E,F) Higher magnification views of CC (E) and CT (F) regions identified in D. (G,H) Experimental scheme used to fate map blastema-derived cartilage regions. (G) Unlabeled vertebrae were implanted into FITC-labeled blastema explants. (H) Resultant CCs/CTs were analyzed for Col2 and Alk Phos expression to identify cartilage regions derived from blastemal cells. (I) Quantification of FITC^{+} areas within Alk Phos^{+} Col2^{+} CC regions and Alk Phos^{-} Col2^{+} CT regions (n=5). *P<0.05; Student's t-test. (J) Representative cultured FITC-labeled blastema sample implanted with unlabeled vertebra and analyzed for FITC, Col2 and Alk Phos expression. (K,L) Higher magnification views of CC (K) and CT (L) regions identified in J. Data are mean±s.d. cc, cartilage callus; ct, cartilage tube; ve, vertebra. Scale bars: 25 µm.

Development (2016) 143, 2946-2957 doi:10.1242/dev.129585

not in proximal Alk Phos^{+} CCs (n=5) (Fig. 7I-L), confirming that CTs, but not proximal cartilage, are derived from blastemas.

Proximal and distal regenerated lizard tail skeletons form independently from distinct cell sources in response to different signals

Our current understanding of early regenerated lizard tail skeletal development as supported by the results presented in this report are presented in Fig. 8. Lizard skeletal regeneration is divided into three main phases: (1) induction (Fig. 8A); (2) proliferation (Fig. 8B); and (3) hypertrophy (Fig. 8C). During the induction phase, proximal CCs form from vertebra periosteal cells in response to Ihh signaling, whereas the distal CT forms from blastemal cells in response to Shh signals from the ependymal tube of the regenerated spinal cord (Fig. 8A). Next, proximal CCs proliferate in response to BMP signaling (Fig. 8B). BMP-6 is produced by the cartilage callus itself, and BMP-2 produced by anterior ends of CTs activates cartilage callus chemotaxis to close gaps between proximal CC and distal CTs, effectively linking original and regenerated tail skeletons. Finally, proximal CCs undergo hypertrophy in response to both Ihh and BMP signals linked to original tail vertebrae (Fig. 8C). Eventually, hypertrophic CC chondrocytes complete endochondral ossification and are replaced by bone.

Comparisons of lizard (*Anolis carolinensis*) and salamander (*Ambystoma mexicanum*) tail regeneration

Several key experiments described in this manuscript were repeated with salamanders to identify similarities and differences between lizard and salamander tail regeneration. First, we sought to determine whether salamander tail regeneration involves the formation of a CC similar to lizards. As described above, the distinction between CC and CT components of regenerated lizard tail skeletons is facilitated by the fact that lizard CC, but not lizard CT, undergoes endochondral ossification. We could not use this technique to determine whether regenerated salamander skeletons included CCs because no portions of regenerated salamander skeletons ossify. So, to focus on vertebrae-derived cartilage in regenerated salamander tails, we took advantage of the dorsoventral patterning exhibited by regenerated salamander skeletons. Blastema-based salamander tail skeletal regeneration is restricted to ventral regenerated salamander tails (Fig. S22A). Thus, to identify vertebral-derived salamander CCs, we focused on cartilage formed in dorsal proximal regenerated salamander tails (Fig. S22B). Dorsal salamander cartilage regions were associated with original tail vertebrae and resembled CC regions of regenerated lizard tails. Identification of dorsal salamander CCs was further validated with ependymal tube removal experiments, similar to those carried out for lizards (Fig. 3). As in lizards, removal of salamander tail ependymal tubes resulted in loss of blastema-derived cartilage (Fig. S22C), and also led to expansion of dorsal salamander CC regions (Fig. S22D).

Although both lizards and salamanders developed CCs, only lizard CCs underwent endochondral ossification. In lizards, proximal CCs associated with original tail vertebrae (Fig. S23A) were converted to bone (Fig. S23A,B). Lizard CC chondrocytes in contact with the terminal vertebra underwent hypertrophy as they enlarged and expressed Alk Phos (Fig. S23C). Periosteum/perichondrium formed

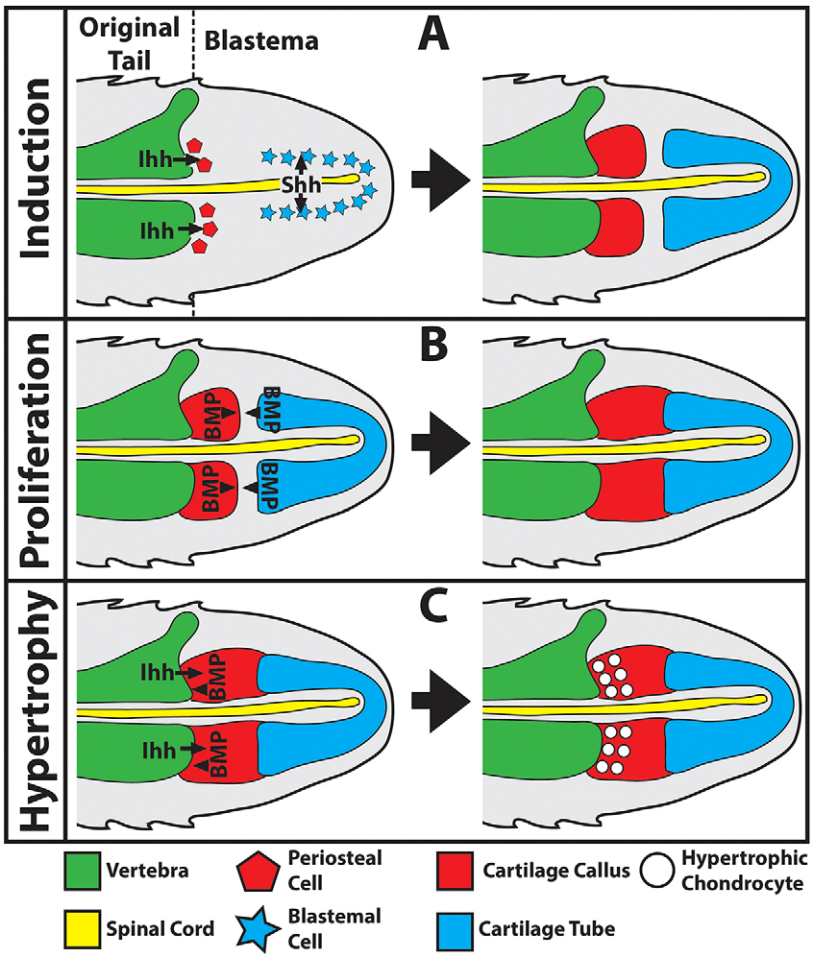

Fig. 8. Summary of cells and signals regulating regenerated lizard tail skeletal development. (A-C) Schematics of sagittal sections of a regenerated lizard tail to highlight cell sources and signals regulating regenerated cartilage induction (A), proliferation (B) and hypertrophy (C). (A) The proximal cartilage callus forms from periosteal cells derived from original tail vertebrae in response to Ihh signaling, whereas the cartilage tube forms from blastemal cells in response to Shh signals from the regenerated spinal cord ependymal tube. (B) The proximal cartilage callus proliferates and expands towards the cartilage tube in response to BMP signaling. (C) The proximal cartilage callus undergoes hypertrophy in response to both Ihh and BMP vertebral signals.

Development (2016) 143, 2946-2957 doi:10.1242/dev.129585

around regions of hypertrophic chondrocytes and expressed Ihh (Fig. S23D), and ossification centers formed in between terminal tail vertebrae and CCs (Fig. S23C,D). Thus, lizard CCs developed growth plate-like organization as they underwent endochondral ossification. This entire process was absent in regenerated salamander tails. Salamander CCs contacted original tail vertebrae similar to lizard CCs (Fig. S23E), but salamander CCs did not undergo endochondral ossification (Fig. S23F), and salamander CC chondrocytes did not enter hypertrophy. There was no evidence of growth plate-like structures in salamander CCs, which also lacked Alk Phos (Fig. S23G) and Ihh (Fig. S23H) expression. We believe that these interesting differences are functionally related to differences in development between lizard and salamander tail skeletons. Original lizard tails develop and grow through endochondral ossification (Fig. S24A), whereas the centrum of the salamander vertebrae remains cartilaginous without transitioning to bone during all life stages (Fig. S24B). Thus, we believe that endochondral ossification processes that occur in lizard, but not salamander, CCs reflect embryonic developmental mechanisms.

Important differences between regenerated lizard and salamander skeletons in terms of dorsoventral patterning were also observed. These differences are obvious when 4-week-old regenerated lizard and salamander tails are viewed in cross-section (Fig. S25A,B). Lizard CTs surround ependymal tubes (Fig. S25A), whereas salamander CRs are ventral to ependymal tubes (Fig. S25B). This lack of dorsoventral patterning in lizard versus salamander tails is mirrored in ependymal tubes of regenerated spinal cords. Lizard ependymal tubes express Shh along their entire circumference and do not express the roof plate/neural crest marker Pax7 (Fig. S25C), whereas salamander ependymal tubes exhibit distinct Shh^{+} floor plate and $Pax7^{+}$ roof plate domains (Fig. S25D). Salamander ependymal tube Shh and Pax7 expression patterns closely resemble those of the embryonic lizard neural tube (Fig. S25E); we hypothesize that this reflects the embryonic nature of the salamander nervous system and plays a role in the divergent dorsoventral patterns of salamander versus lizard regenerated tail skeletons.

DISCUSSION

Unique in the animal kingdom, the lizard CT is an adult skeletal organ that only exists in regenerated lizard tails. This study finds that regenerated lizard tails also generate a CC proximal to the CT, and that these two distinct cartilage regions differ in cell sources and regulatory signals. These conclusions were made possible by virtue of two singular properties of regenerated lizard tail skeletons. First, unlike regenerated salamander tail cartilage, which transitions into segmented vertebral columns, the vast majority of the lizard CT persists unchanged for the lifetime of the lizard/regenerate. Thus, the lizard regenerate lacks segmentation and proximodistally stratified structures other than what is provided by original tail stump tissues at extreme proximal tail regions. Second, we took advantage of the fact that lizard vertebra-derived cartilage (described here as the CC) undergoes hypertrophy, whereas blastema-derived cartilage (which makes up the CT) does not. The combination of these unique characteristics distinguished the regenerated lizard tail skeleton as an ideal model for investigating contributions of stump versus blastema cells and signals to regenerated skeletal tissues. Indeed, the most important finding reported here concerns the differences in cell sources between the proximal and distal regions of regenerated lizard tail skeletons. Ever since the first description of the blastema in 1911 (Fritsch, 1911), the cellular origin of regenerated tissues has been one of the primary questions in regenerative sciences. Studies that have focused on this area have essentially supported one of two hypotheses on blastema/regenerated tissue formation (Stocum, 2002). In the first hypothesis, blastemas form from de-differentiated stumps cells that then re-differentiate to form regenerated tissues. In the second hypothesis, reserve stem/progenitor cells that reside within original tail stump tissues differentiate directly into cell lineages that reconstitute regenerates. The various studies that have been performed, the majority of which focused on muscle regeneration in amputated amphibian limbs, have yielded conflicting conclusions (Echeverri et al., 2001; Hay, 1959; Kragl et al., 2009; Kumar et al., 2004; Lo et al., 1993; Morrison et al., 2006, 2010; Stocum, 2002). Adding to the confusion are recent reports that suggest cellular origins of regenerated tissues vary between species (Sandoval-Guzman et al., 2014). Among regenerative amphibians, newts regenerate muscle in regrown limbs via the first hypotheses involving cell de-differentiation, whereas axolotl salamanders regrow muscle from stem cell populations within stump tissues according to the second hypothesis (Sandoval-Guzman et al., 2014).

Our study shows that, in the case of lizard tail skeletal regeneration, both mechanisms are at play, and that cell sources contributing to regeneration differ by location within the regrown tail. Specifically, proximal regenerated lizard tail skeletons are derived from chondrogenic periosteal stem/progenitor cells of the original tail vertebrae, whereas distal skeletons form from multipotent blastema cells. Here, we made the distinction between cells derived directly from vertebrae and cells derived directly from blastemas. That is not to say populations of blastema cells are not derived from vertebrae. However, our studies have shown that, whatever their initial origins, blastema cells (as defined here) are distinct from progenitor cells found within stump tissues, at least as they relate to skeletal regeneration.

To our knowledge, this study reports the first direct evidence of distinctions in cell origin between proximal and distal skeletal structures and lays the groundwork for investigating whether similar trends exist in other examples of regeneration. For example, salamanders also develop proximal callus-like cartilage regions in their regenerated tail skeletons (Fig. S22). However, unlike lizards, salamander CCs do not undergo hypertrophy and endochondral ossification (Fig. S23). We posit that differences in cartilage development between lizard versus salamander regenerated tail skeletons reflect the evolutionary position of lizards relative to salamanders. Salamander skeletons are evolutionarily primitive compared with those of lizards and exhibit several embryonic characteristics. For example, salamander skeletons are largely cartilaginous and retain notochord throughout adulthood, whereas lizard skeletons are fully formed and ossified. We can imagine that development of the original and regenerated skeletons are related, and that lizard regenerated proximal cartilage ossifies because the original lizard skeleton ossifies, whereas the inability of salamander proximal cartilage to ossify is linked to the absence of endochondral ossification in the original salamander tail. Furthermore, the realities of joining cartilaginous and ossified skeletons may present additional mechanical and structural challenges to the regenerated lizard tail, and the proximal lizard CC may also function as enhanced attachment sites for binding the regenerated and original tail skeletons. These hypotheses are supported by work presented here showing that cartilage regenerated from amputated lizard CTs does not ossify. Future work will be aimed at determining why lizard, but not salamander, proximal cartilage undergoes hypertrophy and endochondral ossification by comparing salamander and lizard periosteal cells and signals.

Development (2016) 143, 2946-2957 doi:10.1242/dev.129585

Differences between the salamander and lizard are not limited to the proximal CC, and this study highlights important differences between distal skeletal elements regenerated by the two animals, particularly as they relate to dorsoventral patterning. Regenerated lizard tail skeletons lack dorsoventral patterning compared with those of salamander. Lizard CTs surround ependymal tubes, whereas salamander tails contain cartilage rods (CRs) ventral to ependymal tubes. Our study complements earlier work with salamanders (Schnapp et al., 2005), and we can now say that both lizard CTs and salamander CRs are induced by Shh signals derived from ependymal tubes of regenerated spinal cords. However, comparisons of spinal cord Shh expression between the two animals indicated that salamander, but not lizard, ependymal tubes are dorsoventrally patterned. Salamander Shh expression is confined to the ventral ependymal tube 'floor plate', whereas lizard Shh is expressed by the entire circumference. The dorsal salamander ependymal tube has also been shown to express neural crest/roof plate markers, such as Pax7 and MSX1, which we have found to be absent in lizard ependymal tubes. Thus, in terms of neural tube patterning, lizard ependymal tubes are entirely made up of cartilage-inductive Shh^{+} 'floor plate'. From this, it is reasonable to conclude that regenerated lizard tail skeletons lack patterning because regenerated lizard tail ependymal tubes lack dorsoventral patterning. Again, this may reflect differences in evolutionary position between lizards and salamanders; neotenic salamanders, the primitive spinal cords of which retain neural tube dorsoventral patterning even as adults, regenerate similarly patterning spinal cords. By contrast, adult lizard spinal cords lose patterning during development and are unable to recreate embryonic patterning during regeneration.

The above discussion has focused on differences between salamander and lizard tail regeneration, but this study has also highlighted important similarities between lizard and salamander regenerated skeletons. For example, neither salamander nor lizard regenerated skeletons ossify. The perichondria of both salamander CRs and lizard CTs calcify, but both regenerated skeletons are decidedly cartilaginous. Thus, we must consider the possibility that, as a rule, blastema-derived axial skeletons simply do not ossify, and perhaps the regenerated lizard tail CT should be considered as a primitive skeleton regenerated by an amniote. Future work will be aimed at exploring this intriguing possibility.

The result that distal, but not proximal, regenerated lizard tail cartilage is derived from blastema cells may be controversial because it has long been thought that lizard tails do not form true blastemas. This view is based on reports from the 1960s published by P. G. Cox highlighting differences between the early regenerated lizard tail and the classical blastema described from amphibian limb regeneration (Cox, 1969). Our findings reported here have shown that these observations are actually due to differences in limb versus tail regeneration rather than differences between salamanders and lizards, and have little bearing on blastema classification. For example, according to Cox, salamander limb blastema cell proliferation is apically associated with the wound epidermis, whereas lizard cell proliferation centers more proximally (Cox, 1969). With the results from this report, this difference can now be explained by the divergent locations of Shh-producing organization centers in limb versus tail regeneration. Since the report by Cox, numerous studies have demonstrated apical salamander regenerating limb wound epidermis as the source of Shh signals responsible for organizing blastema cell proliferation and differentiation (Imokawa and Yoshizato, 1997; Roy and Gardiner, 2002; Torok et al., 1999). In this article, we show that in the regenerating lizard tail it is the spinal cord ependymal tube, not the wound epidermis, that is the source of Shh signals. This mirrors what has been described for ependymal tube-derived Shh signals regulating differentiation and proliferation in regenerated salamander tail blastemas. Thus, differences in lizard versus salamander blastema descriptions observed in previous studies are more a reflection of the differences in Shh signaling sources, and the true distinction to be made is between limb and tail blastemas rather than excluding early lizard tail regenerates from classification as blastemas.

Earlier studies have also refrained from classifying early regenerated lizard tails as true blastemas due to lack of evidence indicating tail stump cell de-differentiation, which, at the time, was held as a key trait of blastema cell origination. More recent experiments have demonstrated that even the classical blastema cells described for axolotl salamander limbs are derived from resident stem cells rather than de-differentiated pluripotent cells (Sandoval-Guzman et al., 2014), casting the appropriateness of some traditional requirements of blastema classification into doubt. In addition, earlier lizard studies assumed that all regenerated lizard tail tissues, including cartilage, were formed either directly from stump skeletal cells or from undifferentiated reserve stem cells. In light of the results presented here indicating two distinct cell sources for regenerated cartilage, we believe that these earlier reports made assumptions for the whole of the lizard CT based on observations concerning proximal, but not distal, cartilage regions. For example, the results presented by Cox (1969) match our observations of regenerated lizard tail proximal CC regions, which are derived directly from chondrogenic periosteal cells of the original tail vertebrae. However, our work with distal cartilage, particularly experiments concerning spinal cord implants, show that the CT originates from a separate, blastemal cell population capable of differentiating into either cartilage or muscle, and perhaps other lineages. In this regard, our study also challenges the prevailing theory of blastema cell plasticity during regeneration. Work done with salamander limbs has unequivocally shown that, under normal circumstances, blastema cells retain lineage-restricted differentiation capabilities during regeneration (Kragl et al., 2009). For example, blastema cells derived from original limb muscle give rise to regenerated muscle tissue. However, these salamander studies did not test whether muscle-derived blastemal cells could differentiate into cartilage cells in artificially manipulated regeneration circumstances. Our experiments demonstrating ectopic CT induction by spinal cord implants showed that lizard blastema cells exhibit some degree of plasticity or transdifferentiation, at least as they pertain to cartilage and muscle differentiation. In these experiments, spinal cord implants induced chondrogenesis in blastema cells that would otherwise have differentiated into muscle. Having identified Shh as the factor responsible for inducing chondrogenesis in lizard blastemal cells, it is tempting to speculate that, in the absence of Shh stimulation, lizard blastema cells default towards the muscle lineage. Future work will be aimed at testing this hypothesis and at defining the differentiation capacities of lizard blastema cell lineages.

In conclusion, this study demonstrates that proximal and distal regenerated lizard tail skeletal regions form independently from different cell sources and in response to different signals. The proximal skeleton is directly derived from periosteum from the original tail vertebrae and resembles a CC formed during fracture repair, whereas the distal CT is derived from the blastema similar to the salamander regenerated tail. Therefore, we propose referring to the proximal cartilage region as the proximal CC, rather than CT,

Development (2016) 143, 2946-2957 doi:10.1242/dev.129585

to reflect its independence from the true, blastema-derived CT. In challenging several long-held assumptions, particularly related to blastema formation and cell sources of regenerated lizard tail cartilage, this study also provides a much needed update on the mechanisms and cell populations regulating lizard skeletal regeneration. In doing so, this report places lizard tail regeneration in better context with modern observations on mammalian fracture healing and amphibian limb/tail regeneration, highlighting common themes as well as important distinctions that result in very different regenerative outcomes. In the end, the findings suggest that lizards, evolutionarily intermediate to amphibians and mammals, employ an amalgam of lower and higher vertebrate wound healing responses during tail skeletal regeneration, hinting at an evolutionary role in regenerative outcomes.

MATERIALS AND METHODS

Lizard tail blastema surgical manipulations and explant culture

Lizard (*Anolis carolinensis*) tail blastemas (Fig. S1) were subjected to surgical procedures prior to embedding in Col1 gels. All surgical manipulations were performed under observation with an Olympus SZX16 dissecting microscope. Tissue to be manipulated was soaked in HBSS supplemented with Antibiotic-Antimycotic (Life Technologies). See supplementary Materials and Methods for specific details on surgical manipulations, including CT and regenerated spinal cord isolation (Fig. S2), spinal cord transplantation (Fig. S3), ependymal tube removal (Fig. S4) and CT relocation (Fig. S5), as well as descriptions of lizard tail blastema explant culture.

Lizard cell culture isolation and culture

Cells were isolated from lizard tail blastemas, periosteum, CCs and CTs, as well as from chicken embryonic limb buds, and cultured *in vitro*. See supplementary Materials and Methods for specifics on cell isolations and culture conditions.

Drug and growth factor treatments

Lizard tail blastema explants were treated with LBEM supplemented with 600 nM cyclopamine (LC Laboratories), 40 nM SAG [N-methyl-N′-(3-pyridinylbenzyl)-N′-(3-chlorobenzo[b]thiophene-2-carbonyl)-1,4-diaminocyclohexane] (Stem RD), 75 ng/ml noggin, (Peprotech), 100 ng/ml BMP-2 (Peprotech) or vehicle control (PBS or ethanol). In experiments involving beads, AG1-X2 resin beads (Bio-Rad) were soaked in either 20 mg/ml cyclopamine, 2.5 mg/ml SAG or vehicle control (ethanol) overnight at 4°C, washed three times in HBSS, and implanted into the dorsal and/or ventral surfaces of lizard tail blastemas. Comparatively hard resin beads easily slipped under soft blastema epidermis. Explants were cultured as described in the supplementary Materials and Methods. SAG and cyclopamine concentrations used in studies involving SAG treatments to rescue hedgehog signaling inhibition by cyclopamine were determined with titration experiments carried out for both soluble and bead-delivered drugs (Fig. S6).

Histology and immunohistochemistry (IHC)

Lizard tissue samples were analyzed by histology (Movat's pentachrome stain) and IHC exactly as previously described (Lozito and Tuan, 2015). Pentachrome stains cartilage green and bone red/orange, making it the ideal stain for analyzing skeletal regeneration. See Table S1 for IHC antibody specifics and Fig. S7 for validation of collagen type X (Col10) antibodies. All histology/IHC images of sagittal sections are presented dorsal towards the top, ventral bottom, distal right and proximal left.0

Fluorescent labeling of lizard tail tissues

Lizard vertebrae and blastemal tissue were isolated from original and regenerated lizard tails, respectively, washed with HBSS, and incubated in 10 µM carboxyfluorescein diacetate-succinimidyl ester (CFDA-SE; Life Technologies) in HBSS at 37°C for 15 min (Sinha et al., 1994). Labeled lizard tissues were then incubated for another 30 min in label-free LBEM at 37°C to ensure the complete modification of the probe and then washed in HBSS.

Micro-computed tomography (microCT)

Samples were immersed in 70% ethanol and scanned with a vivaCT 40 (Scanco Medical, Switzerland) (resolution, 19 µm; energy, 70 kVp; current, 114 µA).

5-Bromo-2'-deoxyuridine (BrdU) labeling

Lizard blastema explants were treated with 1 µM BrdU (Life Technologies) for 16 hours in culture prior to collection. Explants were then processed for histology, and $BrdU^+$ cells were detected by IHC using anti-BrdU primary antibody (Abcam, ab6326; 1:200).

Migration and proliferation assays

The effects of lizard tissues and/or exogenous growth factors on isolated lizard cell migration and proliferation were measured using the xCELLigence System. See supplementary Materials and Methods for descriptions of the xCELLigence System and experiment specifics. Cell proliferation in lizard cartilage explant cultures were measured with the CellTiter 96 AQueous One Solution Cell Proliferation Assay (MTS) according to the manufacturer's instructions.

Statistics

Results from experimental observations, such as those involving surgical manipulations, are indicated as ratios between numbers of samples yielding positive results and total sample numbers (e.g. 4/5). Cell migration, proliferation, and western blot densitometry measurements for three experimental replicates are expressed as the mean±s.d., and significant differences between control and experimental conditions were determined by two-tailed Student's *t*-tests.

Acknowledgements

We acknowledge helpful comments on the manuscript by Aaron Sun.

Competing interests

The authors declare no competing or financial interests.

Author contributions

T.P.L. designed the research study, performed the experiments, analyzed the data and wrote the paper. R.S.T. acted as mentor to T.P.L., aided in developing the experimental approach and interpreting the results, and revised and edited the paper.

Funding

This project was supported by the Pennsylvania Department of Health [SAP 4100050913]; and the National Institutes of Health [R01 GM115444]. Deposited in PMC for release after 12 months.

Supplementary information

Supplementary information available online at
http://dev.biologists.org/lookup/doi/10.1242/dev.129585.supplemental

References

Alibardi, L. (2010). Morphological and cellular aspects of tail and limb regeneration in lizards. A model system with implications for tissue regeneration in mammals. *Adv. Anat. Embryol. Cell Biol.* **207**, iii, v-x, 1-49.

Bai, X., Wang, Y., Man, L., Zhang, Q., Sun, C., Hu, W., Liu, Y., Liu, M., Gu, X. and Wang, Y. (2015). CD59 mediates cartilage patterning during spontaneous tail regeneration. *Sci. Rep.* **5**, 12798.

Bellairs, A. D. and Bryant, S. V. (1985). Autotomy and regeneration in reptiles. In *The Biology of The Reptilia*, Vol. 15 (ed. F. Billet and C. Gans), pp. 303-410. New York: John Wiley & Sons, Inc.

Cox, P. G. (1969). Some aspects of tail regeneration in the lizard, Anolis carolinensis .I. A description based on histology and autoradiography. *J. Exp. Zool.* **171**, 127-149.

Echeverri, K., Clarke, J. D. W. and Tanaka, E. M. (2001). In vivo imaging indicates muscle fiber dedifferentiation is a major contributor to the regenerating tail blastema. *Dev. Biol.* **236**, 151-164.

Fisher, R. E., Geiger, L. A., Stroik, L. K., Hutchins, E. D., George, R. M., Denardo, D. F., Kusumi, K., Rawls, J. A. and Wilson-Rawls, J. (2012). A histological comparison of the original and regenerated tail in the green anole, Anolis carolinensis. *Anat. Rec. Adv. Integr. Anat. Evol. Biol.* **295**, 1609-1619.

Fritsch, C. (1911). Experimentelle studien uber regenerations-vorgange des gleidmassenskeletts der amphibien. *Zool. Jqhrb Abt. Allg. Zool. Physiol.* **30**, 377-472.

Development (2016) 143, 2946-2957 doi:10.1242/dev.129585

Hay, E. D. (1959). Electron microscopic observations of muscle dedifferentiation in regenerating amblystoma limbs. *Dev. Biol.* **1**, 555-585.

Holtzer, S. (1956). The inductive activity of the spinal cord in urodele tail regeneration. *J. Morphol.* **99**, 1-39.

Hutchins, E. D., Markov, G. J., Eckalbar, W. L., George, R. M., King, J. M., Tokuyama, M. A., Geiger, L. A., Emmert, N., Ammar, M. J., Allen, A. N. et al. (2014). Transcriptomic analysis of tail regeneration in the lizard anolis carolinensis reveals activation of conserved vertebrate developmental and repair mechanisms. *PLoS ONE* **9**, e105004.

Imokawa, Y. and Yoshizato, K. (1997). Expression of Sonic hedgehog gene in regenerating newt limb blastemas recapitulates that in developing limb buds. *Proc. Natl. Acad. Sci. USA* **94**, 9159-9164.

Kragl, M., Knapp, D., Nacu, E., Khattak, S., Maden, M., Epperlein, H. H. and Tanaka, E. M. (2009). Cells keep a memory of their tissue origin during axolotl limb regeneration. *Nature* **460**, 60-65.

Kumar, A., Velloso, C. P., Imokawa, Y. and Brockes, J. P. (2004). The regenerative plasticity of isolated urodele myofibers and its dependence on Msx1. *PLoS Biol.* **2**, e218.

Lo, D. C., Allen, F. and Brockes, J. P. (1993). Reversal of muscle differentiation during urodele limb regeneration. *Proc. Natl. Acad. Sci. USA* **90**, 7230-7234.

Lozito, T. P. and Tuan, R. S. (2015). Lizard tail regeneration: regulation of two distinct cartilage regions by Indian hedgehog. *Dev. Biol.* **399**, 249-262.

Morrison, J. I., Lööf, S., He, P. P. and Simon, A. (2006). Salamander limb regeneration involves the activation of a multipotent skeletal muscle satellite cell population. *J. Cell Biol.* **172**, 433-440.

Morrison, J. I., Borg, P. and Simon, A. (2010). Plasticity and recovery of skeletal muscle satellite cells during limb regeneration. *FASEB J.* **24**, 750-756.

Rinkevich, Y., Lindau, P., Ueno, H., Longaker, M. T. and Weissman, I. L. (2011). Germ-layer and lineage-restricted stem/progenitors regenerate the mouse digit tip. *Nature* **476**, 409-413.

Roberts, S. J., van Gastel, N., Carmeliet, G. and Luyten, F. P. (2015). Uncovering the periosteum for skeletal regeneration: the stem cell that lies beneath. *Bone* **70**, 10-18.

Roy, S. and Gardiner, D. M. (2002). Cyclopamine induces digit loss in regenerating axolotl limbs. *J. Exp. Zool.* **293**, 186-190.

Sandoval-Guzmán, T., Wang, H., Khattak, S., Schuez, M., Roensch, K., Nacu, E., Tazaki, A., Joven, A., Tanaka, E. M. and Simon, A. (2014). Fundamental differences in dedifferentiation and stem cell recruitment during skeletal muscle regeneration in two salamander species. *Cell Stem Cell* **14**, 174-187.

Schnapp, E., Kragl, M., Rubin, L. and Tanaka, E. M. (2005). Hedgehog signaling controls dorsoventral patterning, blastema cell proliferation and cartilage induction during axolotl tail regeneration. *Development* **132**, 3243-3253.

Stewart, S. and Stankunas, K. (2012). Limited dedifferentiation provides replacement tissue during zebrafish fin regeneration. *Dev. Biol.* **365**, 339-349.

Stocum, D. L. (2002). Regenerative biology and medicine. *J. Musculoskelet. Neuronal Interact.* **2**, 270-273.

Torok, M. A., Gardiner, D. M., Izpisua-Belmonte, J.-C. and Bryant, S. V. (1999). Sonic hedgehog (shh) expression in developing and regenerating axolotl limbs. *J. Exp. Zool.* **284**, 197-206.

Wang, Q., Huang, C., Zeng, F., Xue, M. and Zhang, X. (2010). Activation of the Hh pathway in periosteum-derived mesenchymal stem cells induces bone formation in vivo: implication for postnatal bone repair. *Am. J. Pathol.* **177**, 3100-3111.

Wang, Q., Huang, C., Xue, M. and Zhang, X. (2011). Expression of endogenous BMP-2 in periosteal progenitor cells is essential for bone healing. *Bone* **48**, 524-532.

Supplementary Materials

SUPPLEMENTARY METHODS

Lizard Tail Blastema Explant Culture

Lizard (*Anolis carolinensis*) tail blastemas were cultured as explants in a system previously used by our laboratory to culture CT explants (Lozito and Tuan, 2015). Lizard tails in the blastema stage of regeneration (10 days post tail loss by autotomy (10 DPA)) were obtained from reptile supply companies (Tails 'n More Pet Services and Underground Reptiles). Tails were swabbed with 70% isopropyl alcohol and soaked in Hank's Balanced Salt Solution (HBSS; Life Technologies) supplemented with 100 units/ml penicillin, 100 µg/ml streptomycin, and 250 ng/ml fungizone antimycotic (Life Technologies) for 30 min. Disinfected tails were trimmed 2 mm proximal to plane of original tail loss, which were easily identified by the abrupt transition from scaled original tail skin to unscaled blastema epidermis (Fig. S1A). When indicated, bead grafting or surgical manipulations (see below) were carried out at this point. Prepped blastemas were vertically positioned (original tail region oriented toward base of 96-well tissue culture plate) in chicken collagen type 1 (Col1) gels (EMD Millipore) and cultured at 30°C in lizard blastema explant medium (LBEM): 1:1 DMEM/Ham's F12 medium (Life Technologies) containing 50 µg/ml ascorbate (Sigma-Aldrich), 40 µg/ml L-proline (Sigma-Aldrich), 0.1 µM dexamethasone (Sigma-Aldrich), and 10 µg/ml insulin-transferrin-selenium (ITS) supplement (Life Technologies). When needed, LBEM was supplemented with various growth factors and/or drugs (see below). Liquid Medium height was adjusted during culture to maintain apical caps of blastema explants at liquid-air interfaces. Explants were cultured for 2 weeks, during which proximal and distal cartilage tube regions developed under control conditions (Fig. S1). At the conclusion of each experiment, tail tissue was extracted from collagen gel and processed for histology and immunostaining (see below). Cartilage formation and hypertrophy were compared between control and experimental conditions.

Lizard tail Blastema Cell Isolation and Culture

Lizard tail blastemas (10 days post tail loss by autotomy (10 DPA)) were collected and washed in HBSS supplemented with 100 units/ml penicillin, 100 µg/ml streptomycin, and 250 ng/ml fungizone antimycotic. Washed blastemas were incubated in 0.1% EDTA/HBSS for 45 min at room temperature with agitation, and epidermis was peeled from each blastema and discarded. Prepared blastemas were then washed extensively in HBSS, minced, and digested in 1 mg/ml trypsin (Sigma-Aldrich) and 1 mg/ml collagenase for 1 hour at 37°C. Blastema cells were collected in lizard blastema cell medium (LBCM) (DMEM/Ham's F12, 2 mM Glutamax, 0.1 µM dexamethasone, 40 µg/ml proline, 50 µg/ml ascorbate, and 10 µg/ml ITS supplement), seeded into V-bottom tissue culture plates (1 million cells per well), and pelleted by centrifugation at 500xg for 5 min. Blastema cell pellets were cultured at 30°C in LBCM for 3 weeks.

Lizard Periosteal Cell Isolation and Culture

Tail vertebrae were isolated from original lizard tails, spinal cords were removed, and vertebrae were trimmed to remove extreme proximal and distal ends. Prepped vertebrae consisted of relatively uniform, hollow vertebral tubes that facilitated

periosteum removal/isolation. Starting at the proximal end, periosteum was gently peeled from the underlying bone with fine-tipped forceps. Periosteum-free vertebrae were used in experiments testing the origins of the proximal CT. Periosteum pieces were collected and washed with HBSS before plating on tissue culture plastic in DMEM/Ham's F12 medium (Life Technologies) containing 10% fetal bovine serum, 100 units/mL penicillin, 100 µg/mL streptomycin, and 250 ng/mL Fungizone. Over one week of culture at 30°C, periosteal cells crawled out of periosteum pieces, creating "islands" around each piece, and cells were passaged once cell islands began to merge. Cells were collected and plated as micromass cultures according to previous reports (Mello and Tuan, 1999). Micromass cultures were analyzed for Alk Phos expression using the Leukocyte Alkaline Phosphatase Kit (Sigma) according to the manufacturer's instructions and immunostained for Col2.

Lizard Cartilage Callus (CC) and Cartilage Tube (CT) Cell Isolation

Regenerated lizard tails 10 weeks post autotomy and original tails were cut into sections approximately 1 cm in length, and tail sections were dissected with tungsten needles. Collected CCs and CTs were washed with HBSS, minced, and digested in 1 mg/ml trypsin and 1 mg/ml collagenase for 1 hour at 37°C to yield cell suspensions. CC/CT cells were plated on tissue culture plastic and expanded in DMEM/Ham's F12 supplemented with 10% fetal bovine serum, 100 units/mL penicillin, 100 µg/mL streptomycin, and 250 ng/mL Fungizone. Vertebral periosteal cells were isolated as described above. CC, CT, and vertebral cells were mixed 1:20 with unlabeled CC or CT cells and pellet cultured for 3 weeks. To identify CFDA-SE-labeled lizard cells, pellet sections were incubated with alkaline phosphatase-conjugate anti-FITC antibodies (Vector Labs), developed with Vector® Blue alkaline phosphatase substrate, and counterstained with methyl green.

Lizard Tissue-Chick Limb Bud Cell Xenogeneic Co-Cultures

Lizard vertebrae and CTs were isolated from original and regenerated lizard tails, respectively. Chick limb bud cells were isolated from Hamburger-Hamilton stage 23-24 embryonic limb buds digested in 1 mg/ml trypsin and 1 mg/ml collagenase and resuspended in Col1 gels at 20 million cells/ml (DeLise et al., 2000). Lizard vertebrae or CTs (5 mg wet weights) were placed in 96-well plates and covered with 100 µl chick cell/Col1 gel suspensions. Lizard tissue-chick limb bud cell co-cultures were maintained in 1:1 DMEM/F12, 1.1 mM $CaCl_2$, 1% glucose, 10% fetal bovine serum (FBS) (Life Technologies), 2.5 mM β-glycerophosphate, 0.3 mg/ml glutamine, 25 µg/ml ascorbate at 37°C. After 1 week, chick cells degraded and contracted Col1 gels around lizard tissues. After 21 days, co-cultures were collected and analyzed by collagen type X (Col10) immunostaining.

Migration Assays

Migration studies were performed using the Roche xCELLigence System (Limame et al., 2012; Lozito and Tuan, 2014). The system consists of modified Boyden chambers (CIM-Plate 16) with upper and lower chambers separated by a cell-permeable membrane lined with electrodes. Cells are seeded into the top chambers, and candidate chemoattractants are placed in the bottom chambers. As cells migrate across the membrane, they contact electrodes, which the system reads as migrating cells. Lizard CTs (5 mg wet weight), lizard vertebrae (5 mg wet weight), recombinant human BMP-2 (0-100

ng/ml), or negative controls were added to bottom wells, and Lizard periosteal cells (40,000 per well) were added to top wells. Serum-free LBEM was used in all experiments. Plates were scanned every 15 min for 24 hours.

Proliferation Assays

Adherent periosteal cell proliferation experiments were also performed using the xCELLigence System. Here, single-chambered "E-Plates" lined with electrodes were used to monitor cell numbers in real time. As cells proliferate, they contact electrodes, which the system reads as cell proliferation. The small surface area of the 96-well plate set-up combined with high electrode sensitivity makes this system particularly applicable for performing large numbers of replicates with small numbers of cells. Lizard periosteal cells were resuspended to 10000 cells/ml in serum-free LBEM supplemented with 0-100 ng/ml BMP-2, and 100 µl of cell suspensions were added to each well. Plates were scanned every 30 min for 100 hours.

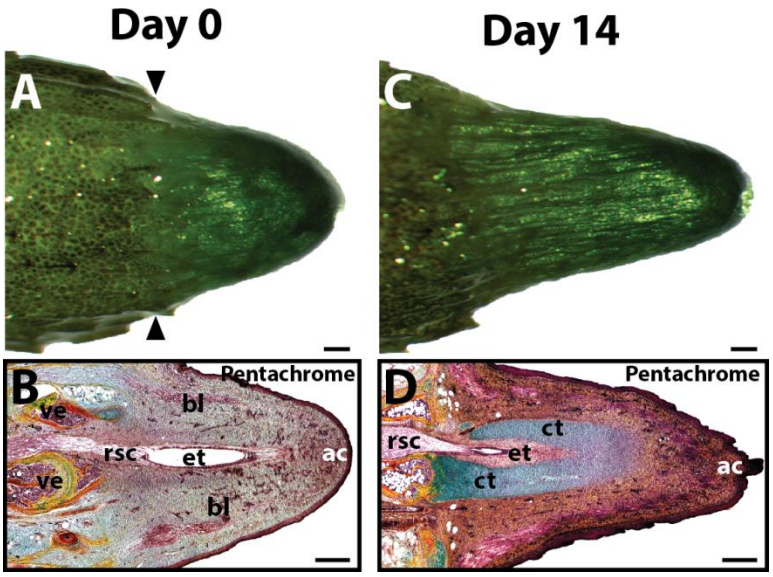

Fig. S1: Lizard tail blastema explant culture. (A) Gross morphology and **(B)** histological analysis (pentachrome) of representative lizard tail blastema isolated for explant culture (Day 0). Black arrow heads mark transition between original tail and blastema. **(C)** Gross morphology and **(D)** histological analysis (pentachrome) of representative lizard blastema at conclusion of explant culture (Day 14). ac, apical cap; bl, blastema; ct, cartilage tube; et, ependymal tube; rsc, regenerated spinal cord; ve, vertebra. Bar = 100 μm.

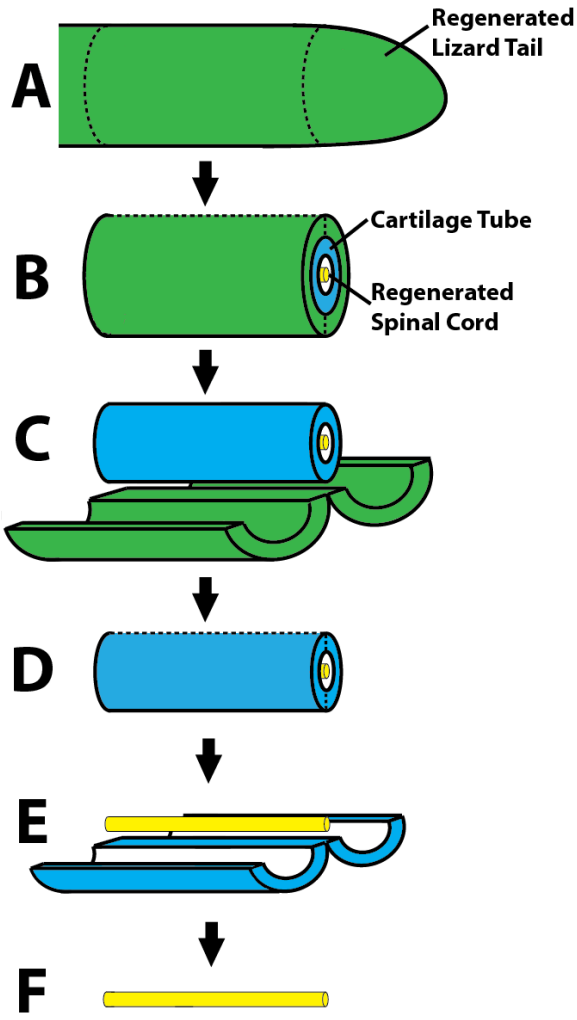

Fig. S2: Schematic of techniques used to isolate CTs and regenerated spinal cords. (A) Regenerated lizard tails (at least 60 DPA) were cut into 5 mm sections. **(B)** Tail sections were cut along the dorsal and ventral midlines down to the depth of the CT. **(C)** Skin, muscle, and connective tissue were laterally peeled to expose CTs. **(D)** In mature regenerates, there exists very little connection between CTs and non-skeletal tissues, and CTs are easily separated from other tail tissues. To isolate regenerated spinal cords, CTs were cut along the dorsal and ventral midlines to the depth of inner CT edge. **(E)** CTs were separated along cut lines. **(F)** Very few tissue connections exist between spinal cords and the CTs, and intact lengths of regenerated spinal cords are easily isolated from remaining CT tissue. Dashed lines denote cut lines.

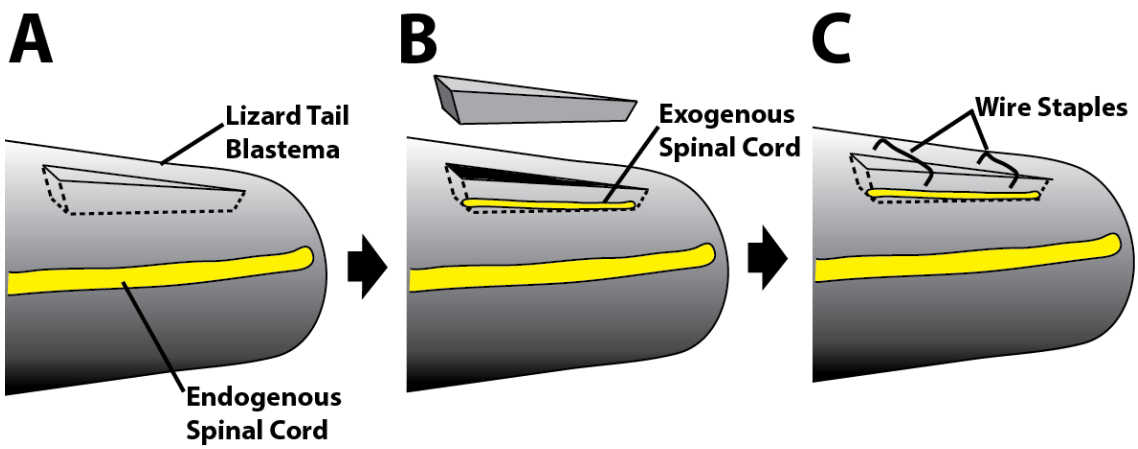

Fig. S3: Schematic of techniques used to transplant exogenous regenerated spinal cords into lizard blastemas. (A) Triangle-shaped incisions 1-2 mm in depth were made on the surfaces of lizard tail blastemas (9-12 DPA). **(B)** Wedge-shaped sections of blastemal tissue gently excised with watch forceps, creating V-bottomed troughs in the blastema. **(C)** Intact regenerated spinal cord pieces extracted from donor regenerated tails (see Fig. S2) were positioned along the bottoms of V-bottomed troughs. **(D)** Wedge-shaped blastemal tissues were replaced into troughs, on top of spinal cord pieces and **(E)** held in place with wire staples. Sham surgery (Control) involved identical steps except spinal cord pieces were omitted. Dashed lines denote cut lines.

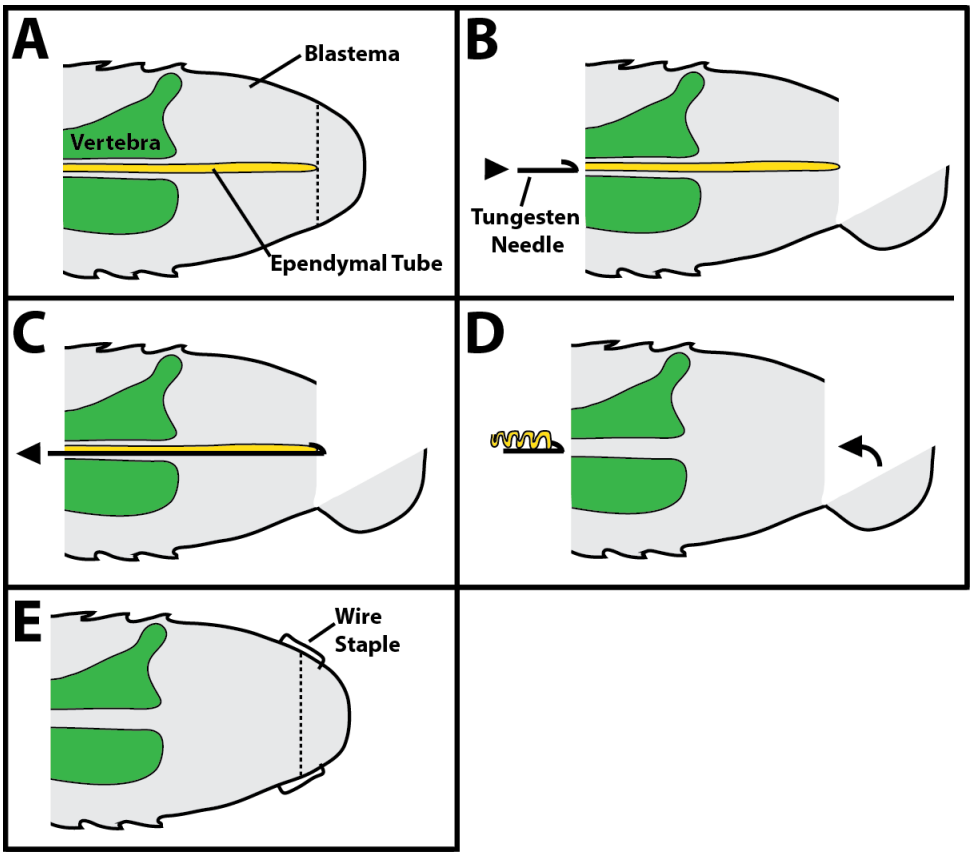

Fig. S4: Schematic of techniques used to remove ependymal tubes from lizard tail blastemas. (A) Lizard tail blastemas (9-12 DPA) with intact original tail vertebrae were cut 1-2 mm from the top. **(B)** Blastemal tips were separated along cut lines, and tungsten needles with tips modified into hooks were inserted into the spinal canals of original tail vertebrae. **(C)** Tungsten needles were guided along spinal canals into blastema tissue until just hooked tips emerged from cut planes. **(D)** The hooked tips were positioned along ependymal tubes, so that when needles were retracted, ependymal tubes were extracted. **(E)** Blastema tips were re-positioned and fixed into place with wire needles. Black arrow heads indicate motion of needles and tissue, and dashed lines denote cut lines.

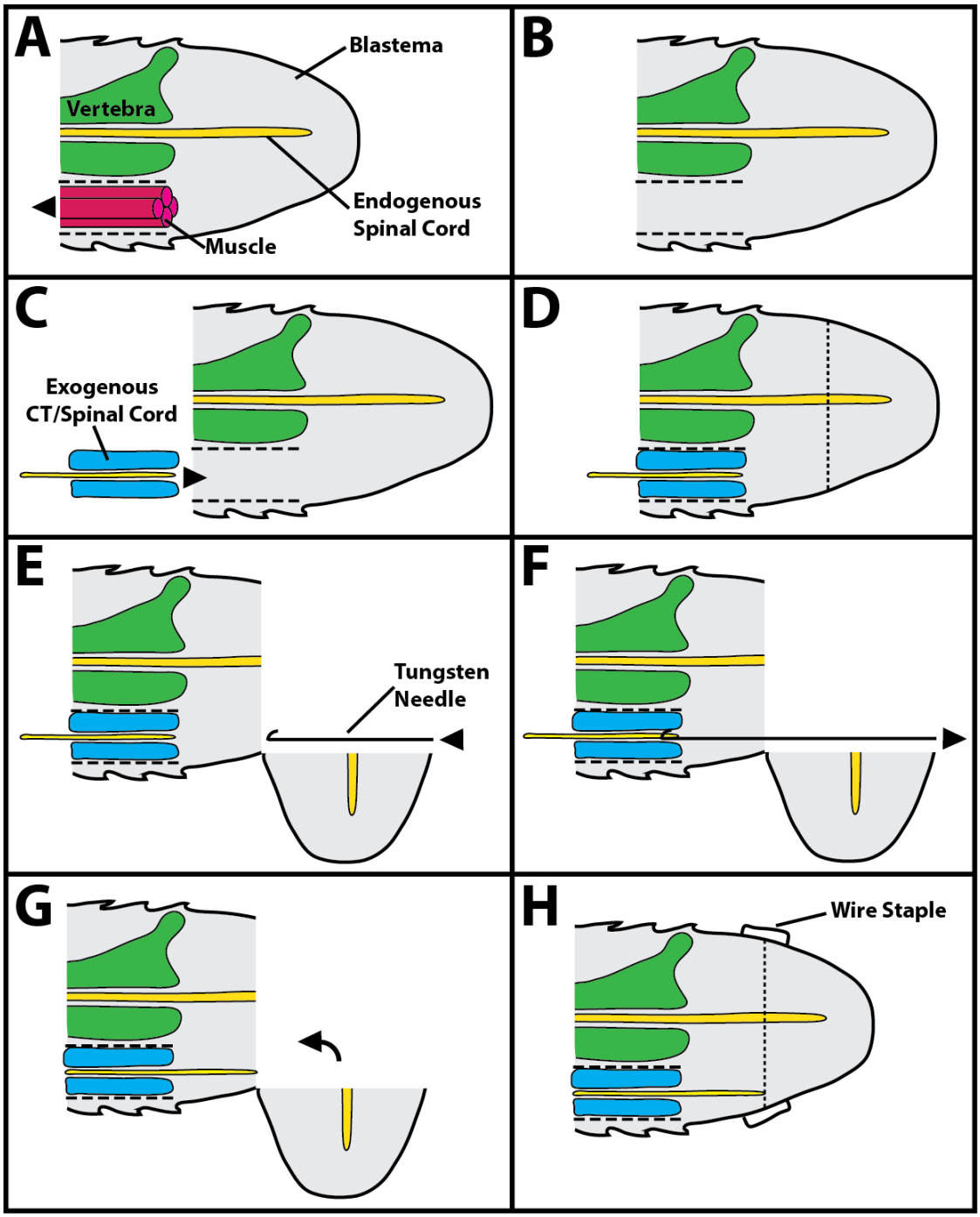

Fig. S5: Schematic of techniques used to relocate distal CTs into proximal tail regions. (A) Lizard blastemas (9-10 DPA) with intact original tail vertebrae were collected, and the connective tissue surrounding one of the ventral tail muscle bundles were cut. **(B)** Dorsal muscle bundle was removed and **(C)** replaced with exogenous CTs containing intact spinal cord isolated from donor regenerated lizard tails (see Fig. S2). **(D)** Blastemas were cut 1-2 mm from the tip. **(E)** Tip regions were separated from blastemas along cut lines. Tungsten needles with modified hooked tips were positioned in line with central canal of inserted CTs. **(F)** Needle tips were inserted into blastemas until hooked tips caught spinal cords of implanted CTs. Needles were retracted along original insertion paths, thereby extending exogenous spinal cords into blastema tissue. **(G)** Blastema tips were repositioned and **(H)** fixed in place with wire staples. Black arrow heads indicate motion of needles and tissue, and dashed lines denote cut lines.

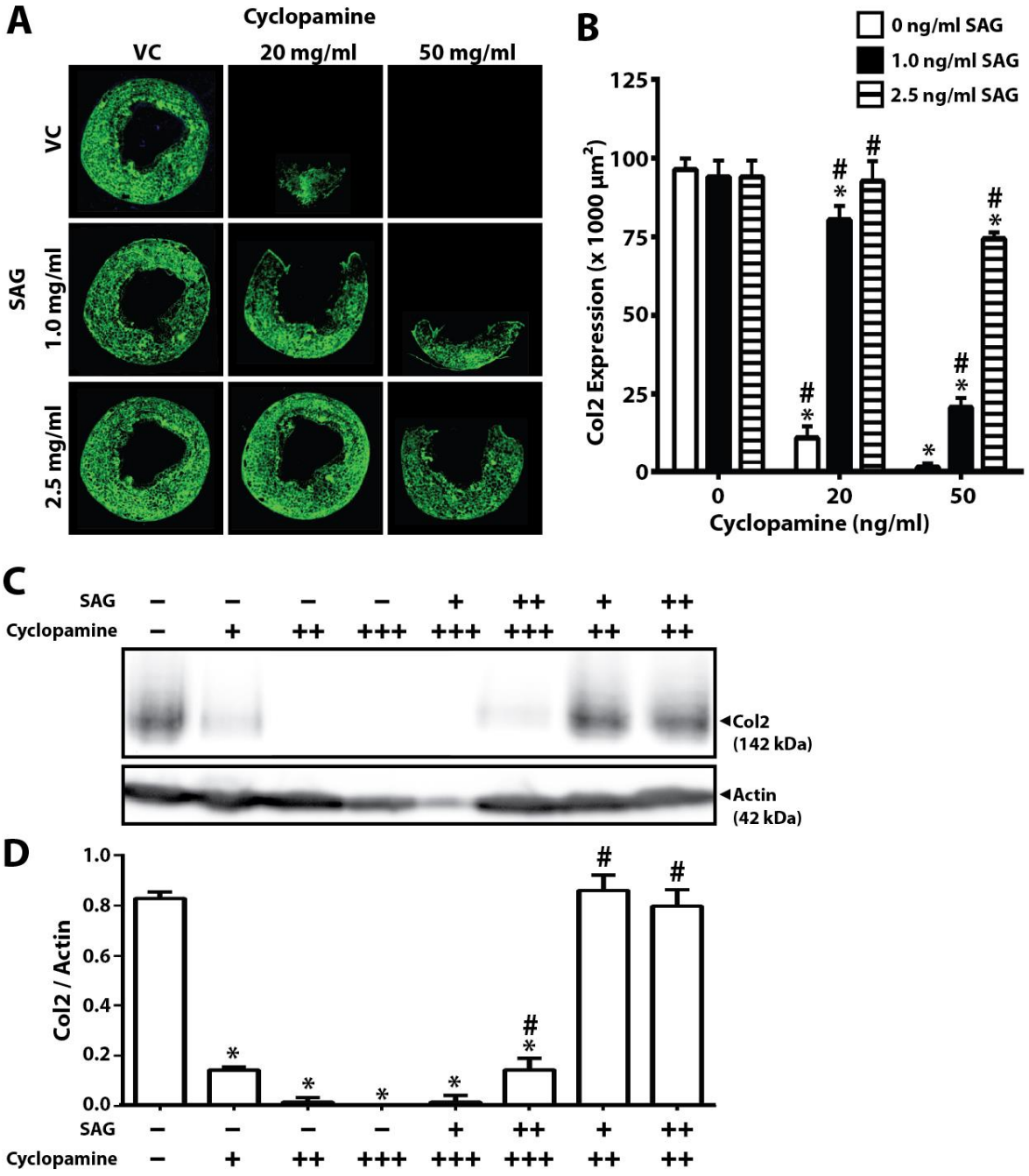

Fig. S6: Titration of cyclopamine and SAG concentrations for modulating lizard tail cartilage formation. (A, B) Titration of cyclopamine/SAG concentration combinations using drug-soaked beads. **(A)** Beads soaked in either vehicle control, cyclopamine (20 or 50 mg/ml), or SAG (2.5 or 1.0 mg/ ml) were implanted in the dorsal surfaces of lizard tail blastemas. These comparatively high drug loading concentrations were necessary due to the low release kinetics exhibited by the resin beads used and the impermeable nature of lizard tail tissues. Following 2 weeks of culture in vivo, blastemas were analyzed by Col2 immunofluorescence. **(B)** Col2 expression for each cyclopamine/SAG-soaked bead concentration combination was quantified as the area of fluorescent signal averaged over three technical replicates (n=3). *, $p < 0.05$ compared to 0 ng/ml cyclopamine condition; #, $p < 0.05$ compared to 0 ng/ml SAG condition. **(C, D)** Titration of cyclopamine/SAG concentration combinations using soluble drugs. **(C)** Lizard tail blastema explants were treated with 0 (-), 300 (+), 600 (++), or 900 (+++) nM cyclopamine and 0 (-), 40 (+), or 80 (++) nM and analyzed by Col2 and actin

Western blots. **(D)** Densitometric analysis of Col2/actin Western blots. Bands from Col2 blots were quantified using ImageJ and normalized to corresponding actin bands. Results are from three experimental replicates (n=3). *, $p < 0.05$ compared to 0 ng/ml cyclopamine condition; #, $p < 0.05$ compared to 0 ng/ml SAG condition.

For bead experiments, 20 mg/ml cyclopamine was sufficient for inhibiting dorsal Col2 expression **(A)**, and 2.5 mg/ml was effective at rescuing cyclopamine-inhibited Col2 expression **(A, B)**. For soluble drug experiments, 600 nM inhibited Col2 expression, while 40 nM SAG rescued Col2 expression **(C, D)**.

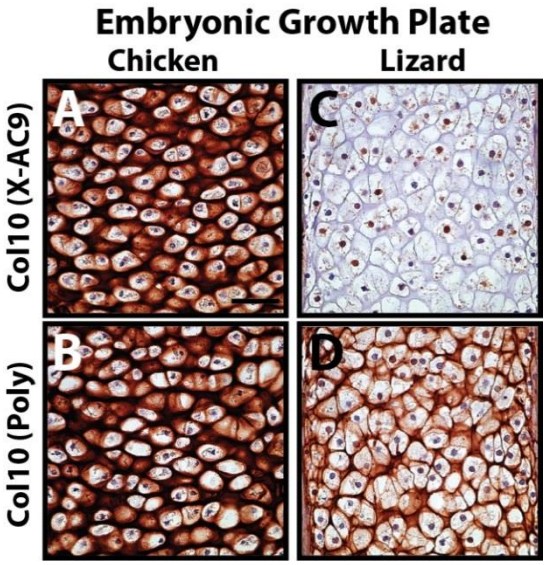

Fig. S7: X-AC9 antibody is specific for chicken, but not lizard, Col10. Growth plates of identically treated **(A, B)** day 11 chick legs and **(B, C)** day 20 embryonic lizard legs (femur) were immunostained using the **(A, C)** X-AC9 monoclonal Col10 antibody or **(B, D)** the polyclonal Col10 antibody (Poly; Abcam ab58632). The X-AC9 antibody reacted with chicken, but not lizard, Col10, while the polyclonal antibody recognized both lizard and chicken Col10. Bar = 50 μm.

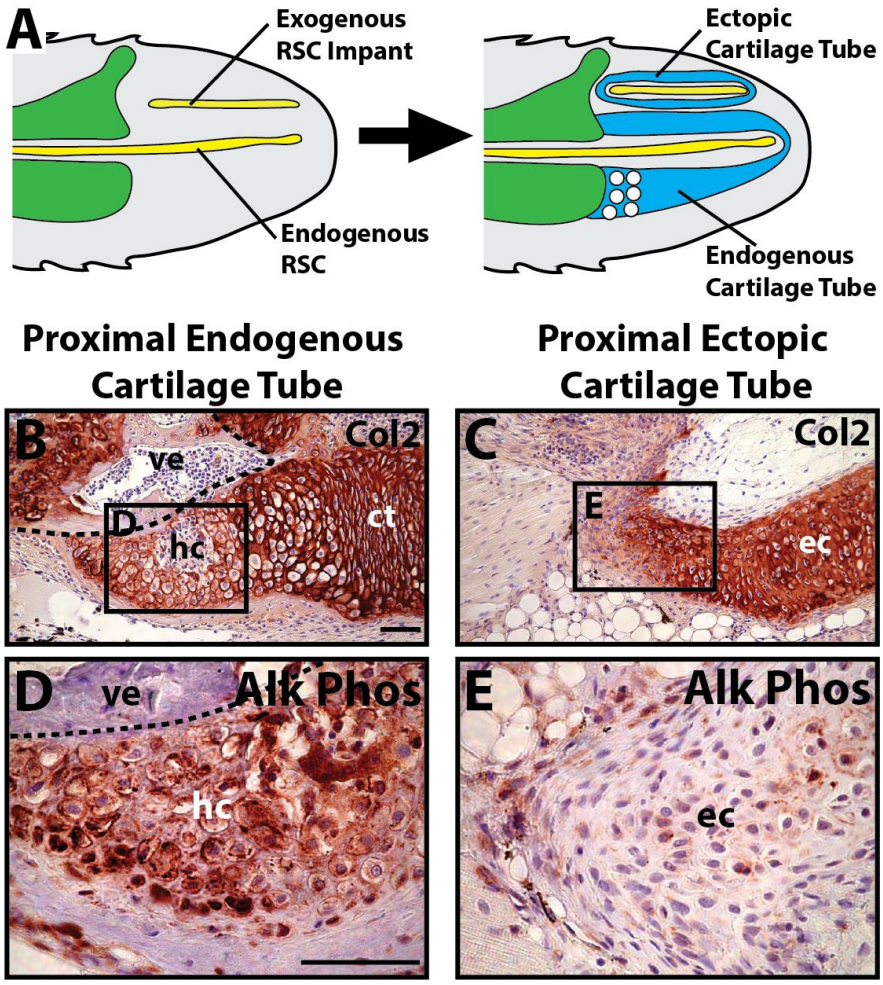

Fig. S8: Proximal lizard cartilage hypertrophy is dependent on the original tail vertebra. (A) Endogenous regenerated spinal cords and exogenous spinal cord implants induce formation of endogenous and ectopic CTs, respectively. However, ectopic and endogenous cartilage differed at their proximal ends, because only proximal endogenous cartilage makes contact with original tail vertebrae. Proximal **(B)** endogenous and **(C)** ectopic cartilage analyzed by Col2 immunostaining. **(D,E)** Higher magnification views of proximal cartilage regions identified in Panels B and C analyzed by Alk Phos immunostaining. Alk Phos+ hypertrophic chondrocytes were only detected in proximal endogenous cartilage areas, which contact the original tail vertebrae. Thus, these results suggested that proximal cartilage hypertrophy is linked to original tail vertebrae. Vertebrae boundaries are traced in dashed lines. ct, cartilage tube; ec, ectopic cartilage tube; hc, hypertrophic chondrocytes; ve, vertebra. Bar = 100 μm.

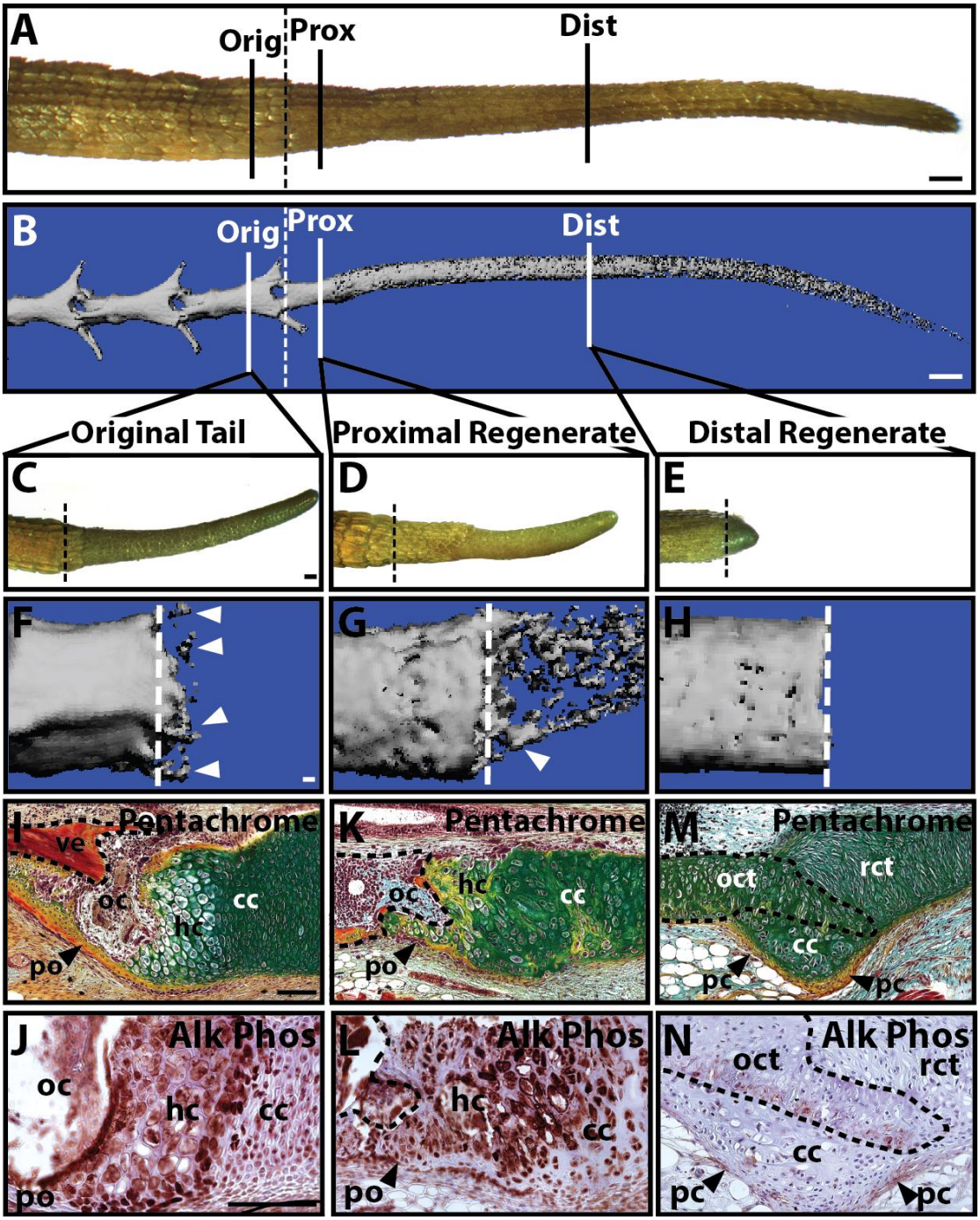

Fig. S9: Lizard tails amputated in osseous, but not cartilaginous, regions, regenerate cartilage that undergoes hypertrophy and endochondral ossification. Results in presented in Figure S6 suggested that proximal cartilage hypertrophy is induced by terminal tail vertebrae. However, what if lizard tails were re-amputated in the regenerated portion? Would the tails "re-regenerate"? If so, would new proximal cartilage regions undergo hypertrophy and ossify without physical interaction with original tail vertebrae? Here we considered these questions and tested whether pro-hypertrophy signals are specific for original tail vertebrae, or if proximal cartilage undergoes hypertrophy and endochondral ossification regardless of the skeletal tissue type present at the amputation site. **(A,B)** Mature lizard tail regenerates with CTs were amputated in (1) the original tail vertebra (Orig), (2) the ossified proximal regenerated tail (Prox), or (3) the partially calcified cartilaginous distal regenerated tail (Dist). In this way, the effects of three different

skeletal tissues (original tail bone, regenerated bone, and CT) on cartilage hypertrophy, endochondral ossification, and overall regeneration were studied. **(A)** Morphological and **(B)** microCT analyses of an intact mature lizard regenerate showing relative position of amputation sites. Following 4 weeks of regeneration, tails amputated in the **(C,F,I,J)** original tail, **(D,G,K,L)** proximal regenerate, or **(E,H,M,N)** distal regenerates were analyzed for **(C-E)** overall regenerate elongation and **(D,H,L)** amputation site ossification. Amputations to **(C)** original (30/n=30) and **(D)** regenerated bone (10/n=10) resulted in sizeable regenerates, while amputations to **(E)** CTs yielded only minimal, stunted regeneration (9/n=10). CTs regenerated from **(F)** original (30/n=10) or **(G)** regenerated osseous regions (10/n=10) exhibited ossification at amputation sites, while **(H)** CTs regenerated from cartilaginous regions did not exhibit any mineralization (10/n=10). **(I-N)** Higher magnification views of amputation sites analyzed by **(I-M)** pentachrome histological staining and (J-N) Alk Phos IHC. **(I,J)** Skeletons regenerated following original tail amputations developed proximal regions that bore striking similarities to CCs formed during fracture healing in higher vertebrates (30/n=30). Here, each CC involved an ossification center bordered by callus borders continuous with the periosteum of the original tail vertebrae and the perichondrium of regenerated skeleton. **(J)** Proximal CCs also developed growth plate-like zones with an abundance of Alk Phos^{+} hypertrophic chondrocyte. **(K,L)** Amputations in ossified proximal regenerated tails also resulted in CCs that ossified and joined the periosteum and perichondrium of osseous and cartilaginous skeletons, respectively (10/n=10). Compared to CCs observed in tails regenerated from amputations to original tail vertebrae, CCs formed from amputations to proximal regenerates exhibited disorganized proximal growth-plate like structures with **(L)** similarly disorganized regions of Alk Phos expression. **(M-N)** Finally, cuts to distal regenerated cartilaginous regions formed CCs that did not develop ossification centers (10/n=10). These CCs were bordered by perichondrium that linked original and regenerated cartilage. Regenerated cartilage did not exhibit growth-plate like zones or hypertrophic chondrocytes and **(N)** did not express Alk Phos (Alk Phos expression was limited to the perichondrium of "old", amputated CTs). In summary, both osseous and cartilaginous skeletons formed CCs in response to amputation, but only CCs developed from osseous tissues developed through hypertrophy and ossification. cc, cartilage callus; hc, hypertrophic chondrocytes; oc, ossification center; oct, original cartilage tube; pc, perichondrium; po, periosteum, rct, regenerated cartilage tube. (A-D) Bar = 0.5 cm, (F-N) Bar = 100 μm.

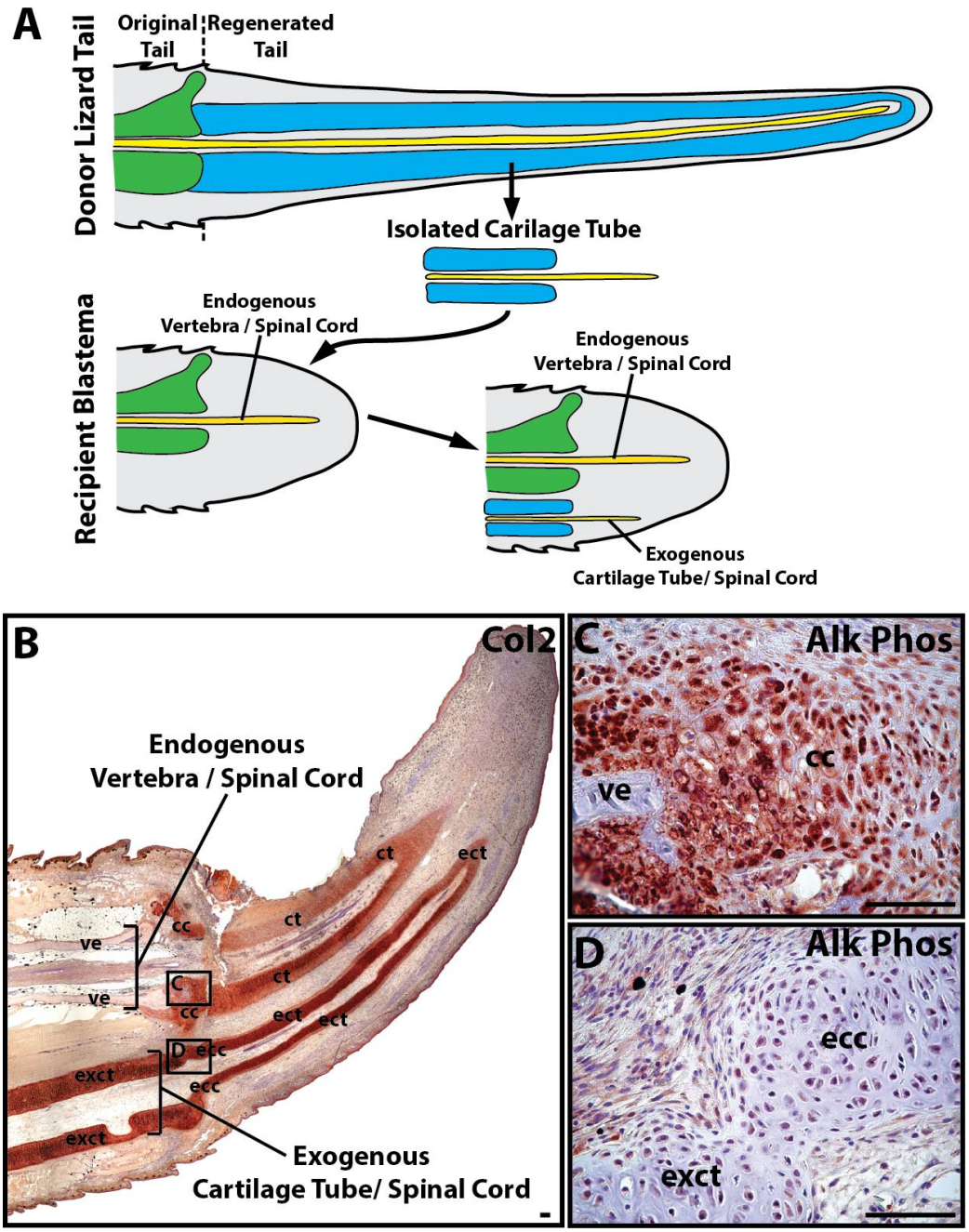

Fig. S10: Proximal cartilage hypertrophy is independent of the proximal lizard tail environment and dependent on original tail vertebrae. The following set of experiments controlled for the distal versus proximal regenerated tail environments and their effects on cartilage development. Our previous studies identified the original tail vertebrae as the candidate source of signals responsible for inducing cartilage hypertrophy and endochondral ossification. But we had not ruled out the original tail muscle, musculature, etc. as possible contributors of pro-hypertrophy signals. Previous studies done in the 1960's demonstrated that CTs with intact spinal cords induced formation of new CTs when implanted into original tail stumps (Simpson, 1964). Here, we sought to repeat these studies with the intention of examining the proximal cartilage areas induced by distal cartilage tube/spinal cord implants. **(A)** CTs with intact spinal cords were isolated from distal regions of donor regenerated tails and implanted into recipient original tail blastemas with endogenous vertebra and spinal cords (see Figure S5 for specifics of surgical manipulations). **(B)** Blastemas 2 weeks following implantation of

exogenous cartilage tube/spinal cord analyzed by Col2 IHC. Endogenous vertebrae and exogenous CTs induced formation of endogenous and ectopic CCs/CTs (4/n=6). Both endogenous and ectopic cartilage contacted skeletal elements within the proximal tail environment. Endogenous proximal cartilage contacted endogenous vertebrae, while ectopic proximal cartilage contacted CT implants. **(C, D)** Higher magnification views of proximal **(C)** endogenous CC and **(D)** ectopic CC regions identified in Panel B analyzed with Alk Phos immunostaining. Cartilage in contact with endogenous vertebrae exhibited hypertrophic morphologies and Alk Phos staining (4/n=4), while ectopic cartilage in contact with CT implants did not develop hypertrophy regions and did not express Alk Phos (4/n=4). These results suggested that vertebrae-derived signals, and not signals derived from other stump/proximal regenerated tail tissues, induce cartilage hypertrophy.

cc, endogenous cartilage callus; ct, endogenous cartilage tube; ecc, ectopic cartilage callus; ect, ectopic cartilage tube; exct, exogenous cartilage tube implant; ve, vertebrae. Bar = 100 μm.

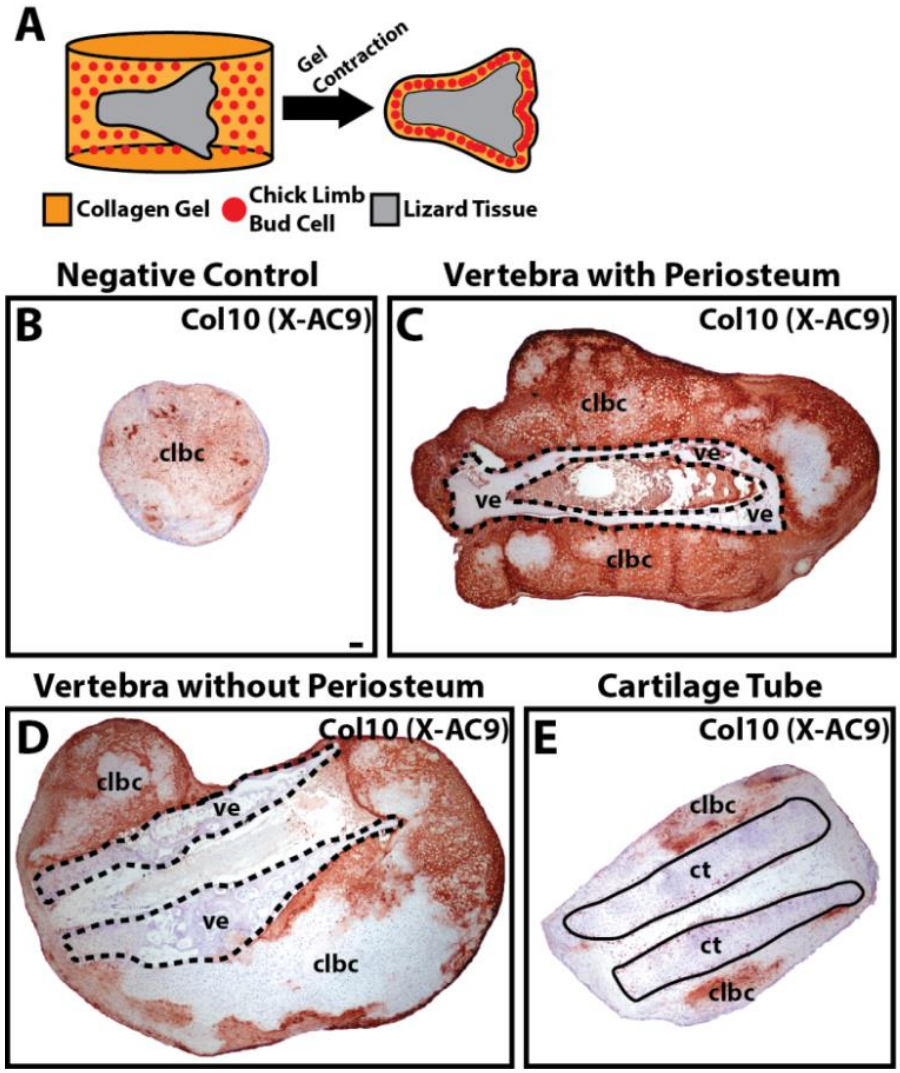

Fig. S11: Lizard vertebrae, but not CTs, induce hypertrophy in chick limb bud mesenchyme. Thus far, results suggested that signals derived from the vertebrae and periosteum induce periosteum-derived cartilage to undergo hypertrophy. However, additional work was needed to elucidate the dependence of proximal cartilage hypertrophy on vertebrae/periosteum signals rather than cells. Addressing this topic posed several technical challenges stemming from difficulties associated with distinguishing between signals and cells derived from the same tissues. To perform these experiments, we took advantage of xenogeneic co-cultures between lizard skeletal tissues and chick limb bud cells. Unlike salamander tissues, lizard tissues survive at the sample temperatures and medium osmolarities as chick and mammalian cells, thereby allowing for co-cultures between lizard tissues and these other cell types. Chick limb bud cells have been extensively used in in vitro models of cartilage development due to the abilities of embryonic limb bud mesenchyme to develop cartilage that undergoes hypertrophy and terminal differentiation under culture (Mello and Tuan, 1999). Adding to the attractiveness of this model is the availability of well-validated, species-specific antibodies to the established cartilage hypertrophy marker Col10. The X-AC9 clone mouse monoclonal antibody recognizes chicken, but not lizard, Col10 (Fig. S7) (Lozito and Tuan, 2015). Thus, xenogeneic lizard-chick co-cultures were used to specifically study the effects of lizard vertebra and periosteum on hypertrophy markers in cartilage formed from chick cells by eliminating contributions from lizard hypertrophic cartilage.

(A) We developed a system for co-culturing chick cells with lizard skeletal tissues in 3-dimensional constructs. Chick cells were suspended in Col1 gels, which were cast over lizard skeletal tissues. Enzymatic and mechanical activities of chick cells caused gels to contract around the lizard tissues within 5 days, allowing for both direct and indirect interactions between lizard tissues and chick cells **(B-E)** After 3 weeks of growth, xenogeneic co-cultures were immunostained for Col10 (X-AC9) to identify chick hypertrophic cartilage regions. **(B)** Negative control samples consisted of chick limb bud cells only, without lizard tissues. Experimental samples involved co-culturing chick cells and **(C)** lizard vertebrae with intact periosteum, **(D)** lizard vertebrae lacking periosteum. **(E)** Co-cultures between lizard distal CTs and chick limb bud cells were included as tissue-type controls. (As presented above, distal CT tissue did not induce hypertrophy in lizard cartilage, and we wanted to validate the relevancy of xenogeneic cultures by testing the effects of lizard CTs on chick cartilage.) In conditions involving lizard vertebrae and CTs, samples included the same amount of lizard tissues (5 mg wet weight). **(C)** Lizard vertebrae induced significant increases in overall cartilage formation and Col10 expression (6/n=6) compared to **(B)** negative and **(E)** lizard CT tissue-type controls. **(D)** Removal of periosteum prior to co-culture did not affect vertebra-induced increases in overall cartilage formation but did significantly decrease Col10 expression (6/n=6) compared to **(C)** vertebra samples with intact periosteum, but not to basal levels seen in **(B)** negative and **(D)** tissue-type control samples. These results confirmed lizard original tail vertebra and periosteum as the sources of pro-cartilage hypertrophy signals.

Dashed lines mark vertebra tissue boundaries, and solid lines trace CT tissue boundaries. clbc, chick limb bud cells, ct, lizard ct, ve, lizard vertebra. Bar = 100 μm.

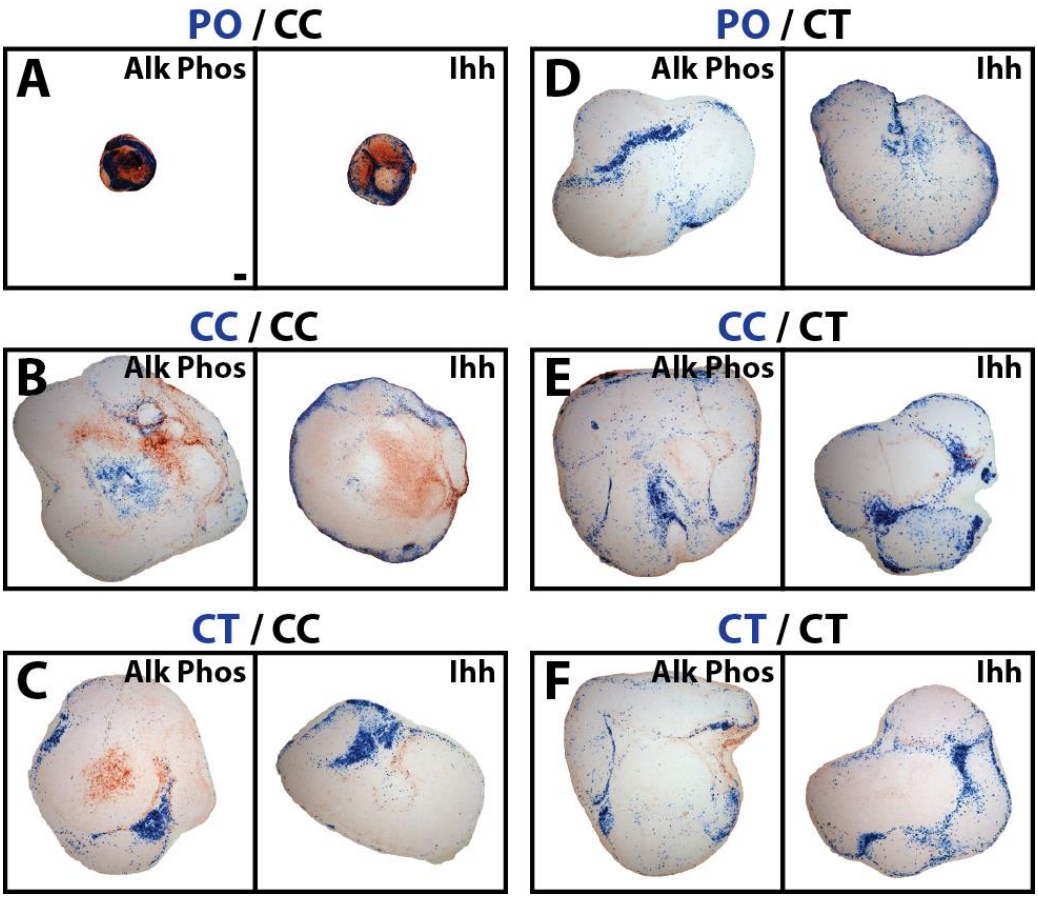

Fig. S12: Lizard periosteal cells induce hypertrophy and Ihh expression in CC, but not CT, cells. (A-F) Lizard periosteal (PO), cartilage callus (CC), and cartilage tube (CT) cells isolated and labeled with CFDA-SE (designated by blue text color in sample titles) and mixed 1:20 with unlabeled CC or CT cells (designated by black text color in sample titles) and pellet cultured for 3 weeks. Samples were co-immunostained for FITC, which stains blue, and either Alk Phos or Ihh, which stains red. **(A)** PO / CC co-cultures were significantly smaller and exhibited higher expression of Alk Phos and Ihh compared to **(B)** CC / CC or **(C)** CT / CC co-cultures. **(D)** PO cells did not affect CT culture size or induce CT Alk Phos or Ihh expression, and, overall, **(E, F)** CT cells exhibited minimal Alk Phos expression. Bar = 100 μm.

These results suggest that vertebral periosteal cells induce hypertrophy and Ihh expression in CC, but not CT, cells. These results also confirm the observations that CC, but not CT, cells respond to periosteal cell-derived signals by undergoing hypertrophy.

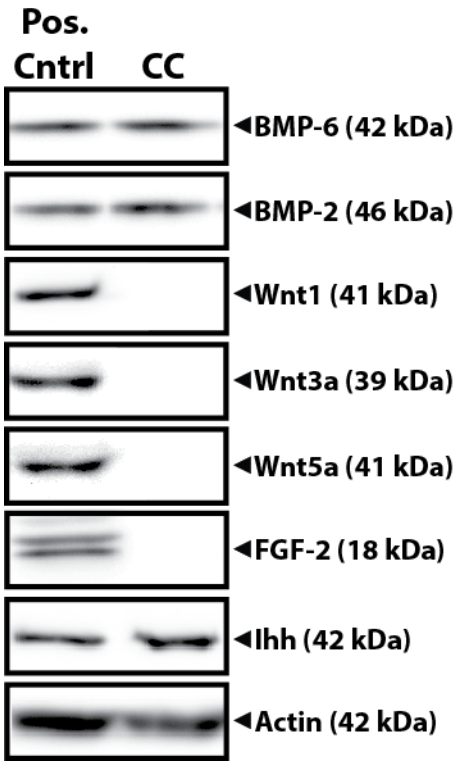

Fig. S13: Analysis of growth factors present in lizard tail CC. CC protein was isolated from lizard tails 14 DPA and analyzed by BMP-6, BMP-2, Wnt1, Wnt3a, Wnt5a, FGF-2, and Ihh Western blots. Protein samples isolated from embryonic lizard limb buds were included as positive controls.

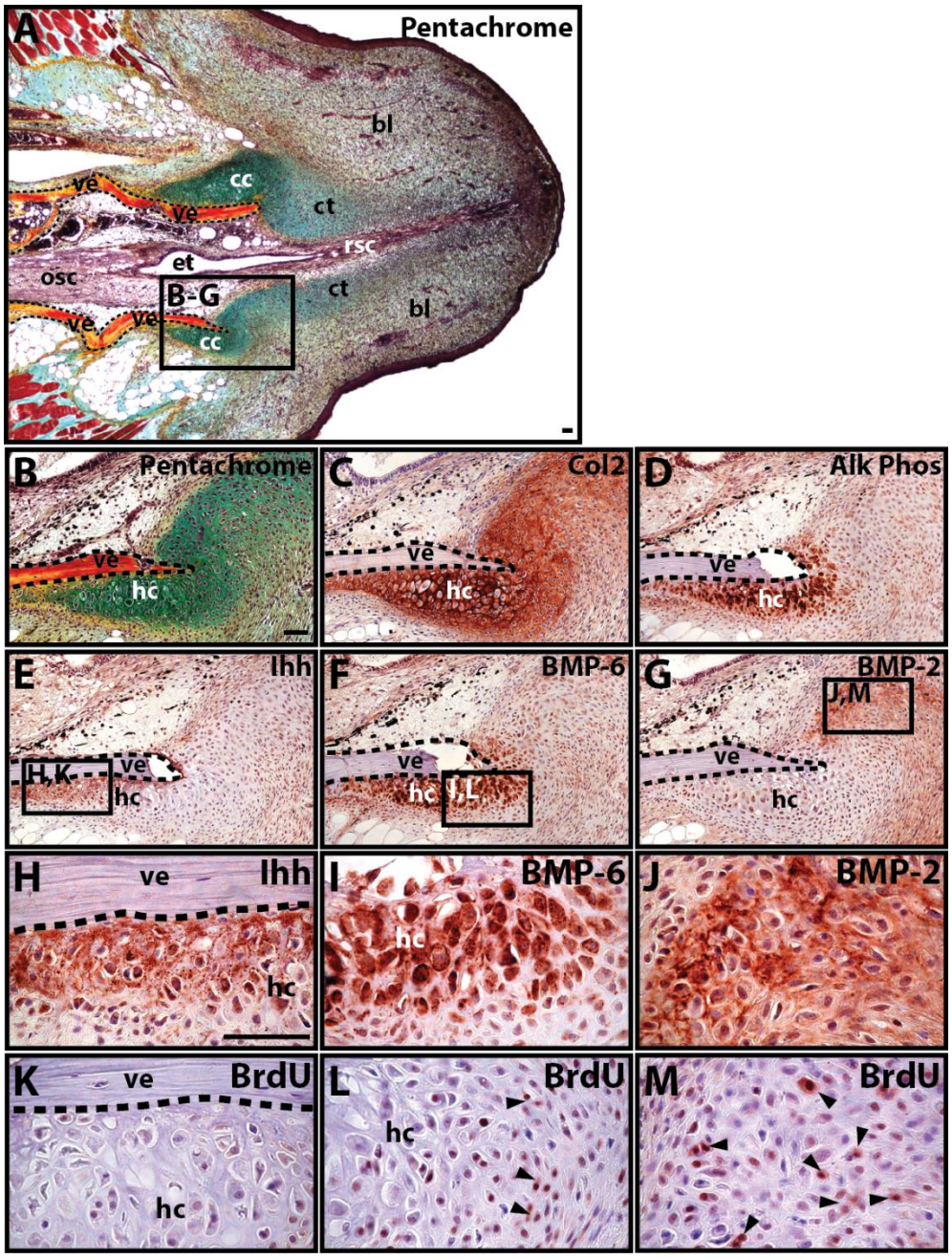

Fig. S14: Proximal cartilage hypertrophy and proliferation localize with Ihh and BMP expression, respectively. In order to study the mechanisms regulating proximal cartilage development, we began by characterizing expression of signaling molecules within the developing proximal cartilage environment. **(A)** Early regenerates (14 DPA) analyzed by pentachrome staining showed initial development of proximal CCs. **(B-I)** Higher magnification views of regions identified in Panel A analyzed by **(B)** histology (pentachrome) or **(C)** Col2, **(D)** Alk Phos, **(E)** Ihh, **(F)** BMP-6, and **(G)** BMP-2 immunostaining. **(H-M)** Higher magnification views of regions identified in Panels E-G. **(K-M)** BrdU immunostaining was used to identify proliferative cells, some of which are identified by black arrow heads. Dashed lines mark vertebral boundaries. bl, blastema; cc, cartilage tube; ct, cartilage tube; et, ependymal tube; hc, hypertrophic chondrocytes; osc, original spinal cord; rsc, regenerated spinal cord; ve, vertebra. Bar = 50 μm

(A) In early regenerates, the majority of the blastemas remained undifferentiated, as evidenced by sparse muscle formation and incomplete glycosaminoglycan deposition by developing CTs. The exception were proximal CCs, which

already exhibited characteristic cartilaginous matrix rich in **(A,B)** glycosaminoglycans and **(C)** Col2. That proximal CCs develop before CTs form from blastemal cells is another clue to their independent formation. **(D)** Proximal CCs contacted terminal tail vertebrae, and these contact regions underwent hypertrophy and expressed Alk Phos. **(E)** Ihh localized to anterior CCs and was highly associated with vertebrae **(H)**, being expressed by both the bone tissue adjacent cartilage regions. **(F)** BMP-6 expression localized to medial CCs and was expressed by hypertrophic chondrocytes **(I)**. **(G)** BMP-2 was expressed by the anterior CC and at the junction between CCs and CTs **(J)**. **(K-M)** BrdU immunostaining was used to identify proliferative cartilage regions. **(K)** Very few proliferative cells were detected in posterior CCs near original tail vertebrae, and the vast majority of proliferative cells were detected in **(L)** medial and **(M)** posterior zones, both of which overlapped with BMP staining **(I,J)**. Thus, these results demonstrated anterior, medial, and posterior localizations of Ihh, BMP-6, and BMP-2 expression, respectively, within regenerated lizard tail CCs. Such findings also linked these signaling molecules with processes of proximal CC development: induction, proliferation, and hypertrophy. Ihh was associated with the vertebrae, which we showed above was involved in proximal CC induction. Proximal cartilage tube proliferation co-localized with BMP-2 and BMP-6 expression, and cartilage hypertrophy overlapped with both Ihh and BMP regions.

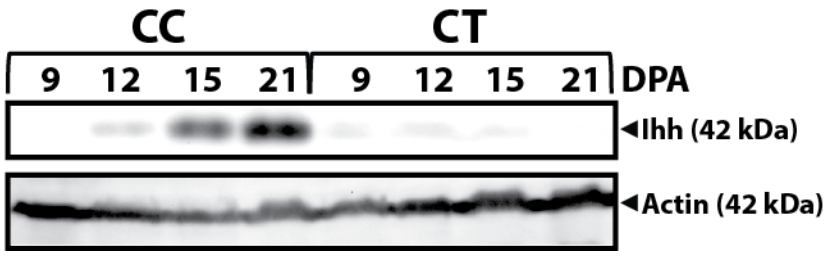

Fig. S15: Time course of CC and CT Ihh expression during early lizard tail regeneration. Protein collected from proximal CC and distal CT regions 9-21 DPA were analyzed by Ihh Western blots.

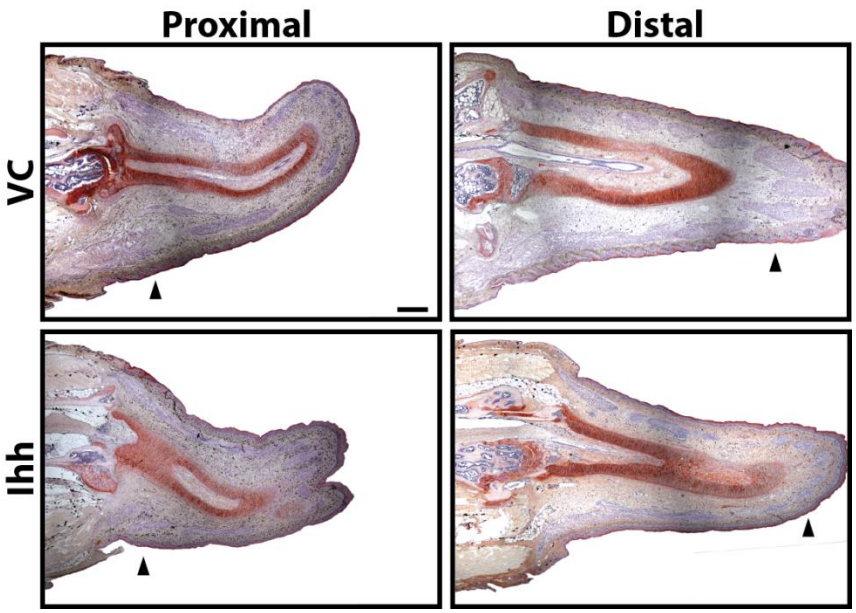

Fig. S16: Ihh-beads do not affect either proximal or distal cartilage formation. Beads soaked in 1mg/ml Ihh or vehicle control (VC) were implanted in the ventral surfaces of either proximal or distal regions of 9 DPA blastemas (implantation sites marked by arrow heads). After two weeks of explant culture, samples were immunostained for Col2. Treatment with Ihh-beads did not significantly affect cartilage formation. Bar = 500 µm.

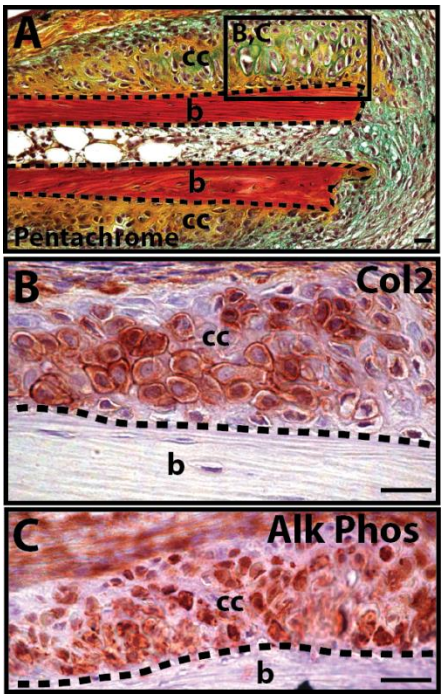

Fig. S17: Cartilage regeneration independent of blastema. (A) Lizard toe 14 days after amputation analyzed by histology (pentachrome). **(B, C)** Higher magnification views of regions identified in Panel A analyzed by **(B)** Col2 and **(C)** Alk Phos immunostaining. Dashed lines mark bone boundaries. b, bone; cc, cartilage callus. Bar = 50 µm.

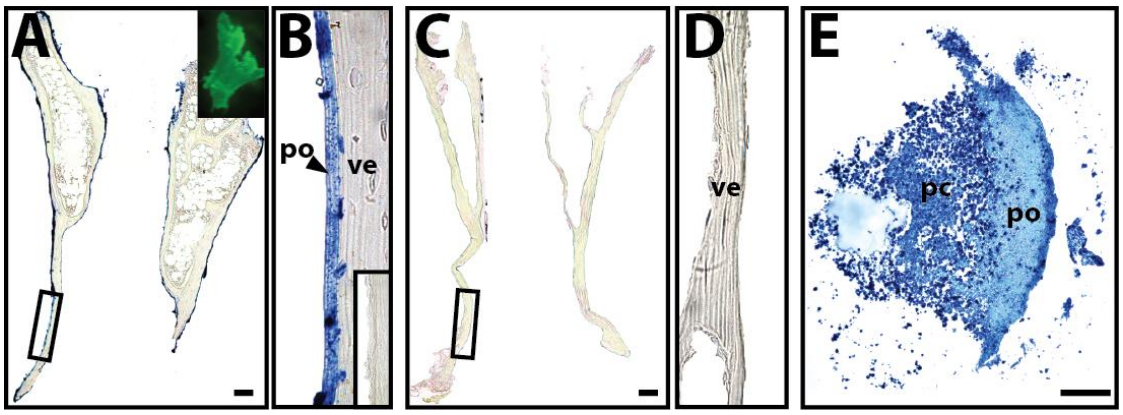

Fig. S18: Selective labeling and isolation of lizard tail vertebra periosteum. **(A)** Sagittal section of a lizard tail vertebra treated with CFDA-SE and analyzed by FITC immunostaining. (Here, distal is directed upwards.) FITC-labeled cells and tissues appear blue. **(A, Inset)** Fluorescence micrograph of CFDA-treated vertebra. **(B)** Higher magnification view of region identified in Panel A highlighting specific FITC labeling of the periosteum. **(B, Inset)** Periosteum of control, unlabeled vertebra. **(C)** Periosteum was removed from CFDA-SE-treated vertebrae, and the remaining tissue was analyzed by FITC immunostaining. **(D)** Higher magnification view of region identified in Panel D demonstrating effective removal of periosteum. **(E)** To validate periosteal cell isolation, periosteal tissue removed from CFDA-SE-treated vertebrae were cultured as explants according to Supplementary Methods for 1 week and analyzed by FITC immunostaining. Cell populations that crawled out of labeled periosteal tissue contained high levels of FITC, indicating enrichment of periosteal cells. pc, periosteal cells; po, periosteum; ve, vertebra. A-E: Bar = 250 μm; F: Bar = 50.

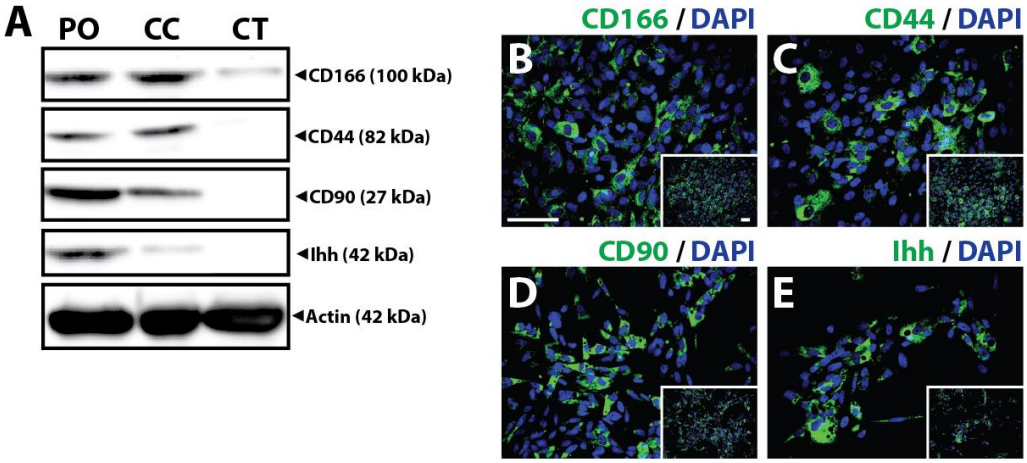

Fig. S19: Lizard periosteal and CC cells express the stem/progenitor cell markers CD166, CD44, and CD90. (A) Cultured cells isolated from lizard periosteal (PO), cartilage callus (CC) and cartilage tube (CT) cells were analyzed by Western blot for expression of the periosteal stem/progenitor cell markers CD166, CD44, and CD90 and for Ihh expression. PO and CC, but not CT, cells expressed high levels of CD166, CD44, and CD90. Only PO cells secreted Ihh in culture. **(B-E)** Periosteal cell expression of CD166, CD44, CD90, and Ihh was validated with immunofluorescence. Bar = 25 μm.

These results identify $CD166^{+}$ $CD44^{+}$ $CD90^{+}$ periosteal stem/progenitor cells as the vertebral source of Ihh, the signal responsible for inducing Alk Phos expression in lizard CC cells. Furthermore, the fact that periosteal markers are also detected in the lizard tail CC further supports the hypothesis that the CC is derived from periosteal cells.

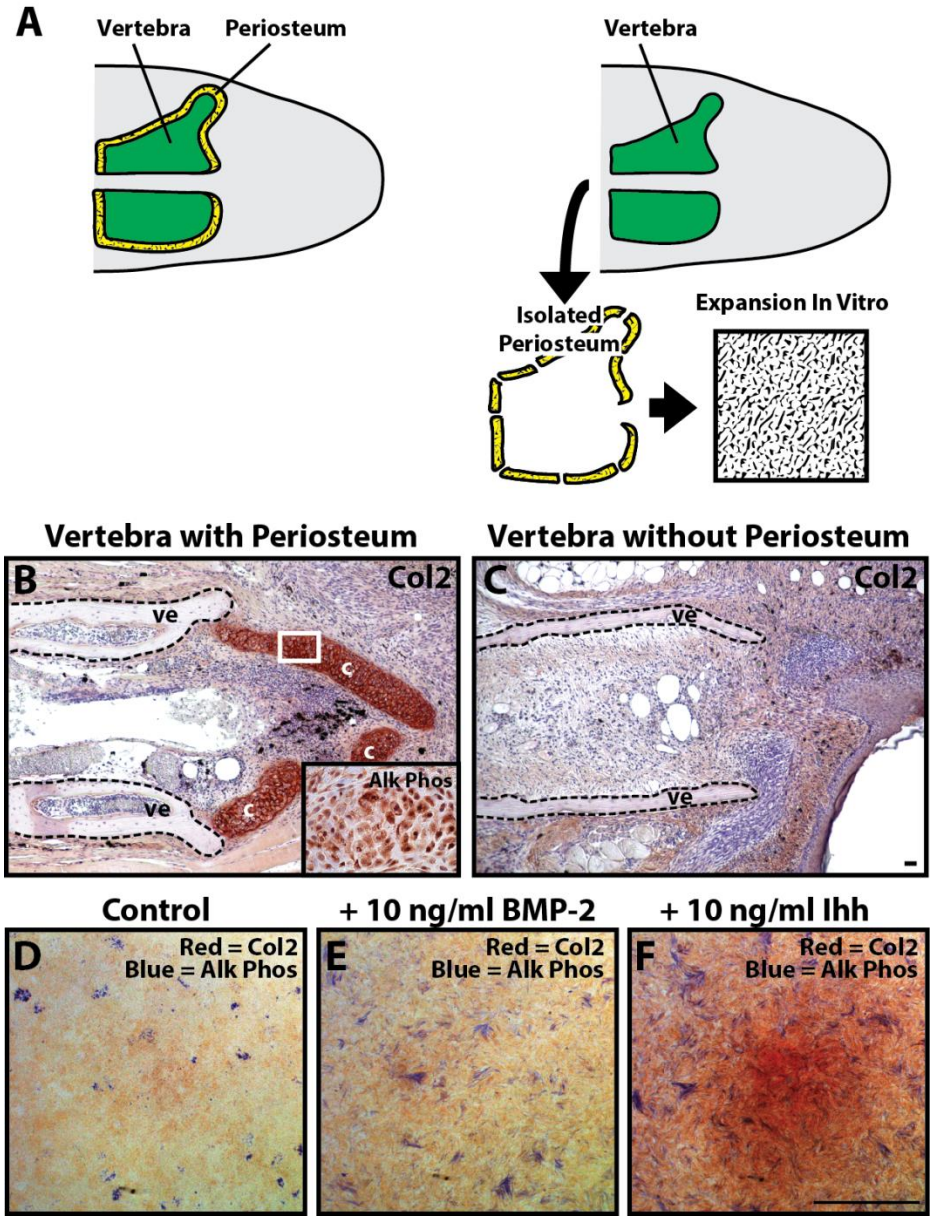

Fig. S20: The proximal regenerated lizard tail skeleton is derived from the periosteum of original tail vertebrae. As presented in Figure S13, the labeling scheme employed in fate-mapping studies preferentially labeled the periosteum of vertebrae (Fig. S13A,B), suggesting that the periosteum is the specific tissue source of the proximal CC. Indeed, the mammalian periosteum is known to harbor populations of stem cells that form CCs during fracture repair (Colnot, 2009). Here we sought to study this directly by testing whether removal of periosteum affected the ability of lizard vertebrae to form cartilage. Periosteum removal was validated, (Fig. S13C,D), and isolated periosteal cells (Fig. S13E) were collected and cultured for experimentation, as described below.

(A) Experimental setup used to investigate role of periosteum in proximal cartilage development. Tails containing vertebrae with intact periosteum and tails containing vertebrae treated to remove periosteum were compared for cartilage formation. Isolated periosteum was used to generate periosteal cells that were expanded in vitro. Spinal cords were also removed from vertebrae/blastemas to focus on vertebra-derived cartilage. **(B)** Vertebrae with intact periosteum formed cartilage (3/n=3) that expressed (3/n=3) Alk Phos **(B, Inset)**, while **(C)** vertebrae without periosteum did not form

cartilage (7/n=7). These results indicated periosteal cells as the source of Alk Phos-expressing cartilage. **(D-F)** For further validation, we performed studies on cells isolated from collected periosteum and tested their responses to hedgehog and BMP signals. Periosteal cell micromass cultures were stained for Alk Phos (Blue) and immunostained for Col2 (Red). **(D)** Populations of perichondral cells cultured under control conditions expressed Alk Phos (3/n=3), while Col2 was undetectable (0/n=3). **(E)** Treatment with 10 ng/ml BMP-2 induced proliferation of Alk Phos-positive cell populations (3/n=3), but Col2 remained undetectable (0/n=3). **(F)** Treatment with 10 ng/ml Ihh stimulated Alk Phos expression and Col2 production. Combined with results from drug/growth factor experiments involving lizard tail blastema explants described in the main article (Fig. 4-6), these results suggested that Alk Phos-positive cartilage of the proximal CC is derived from the perichondrium of vertebrae, and that periosteum-derived cells respond similarly to BMP and hedgehog signaling compared to proximal cartilage.

Dashed lines mark vertebral boundaries. c, cartilage; ve, vertebrae. Bar = 100 μm.

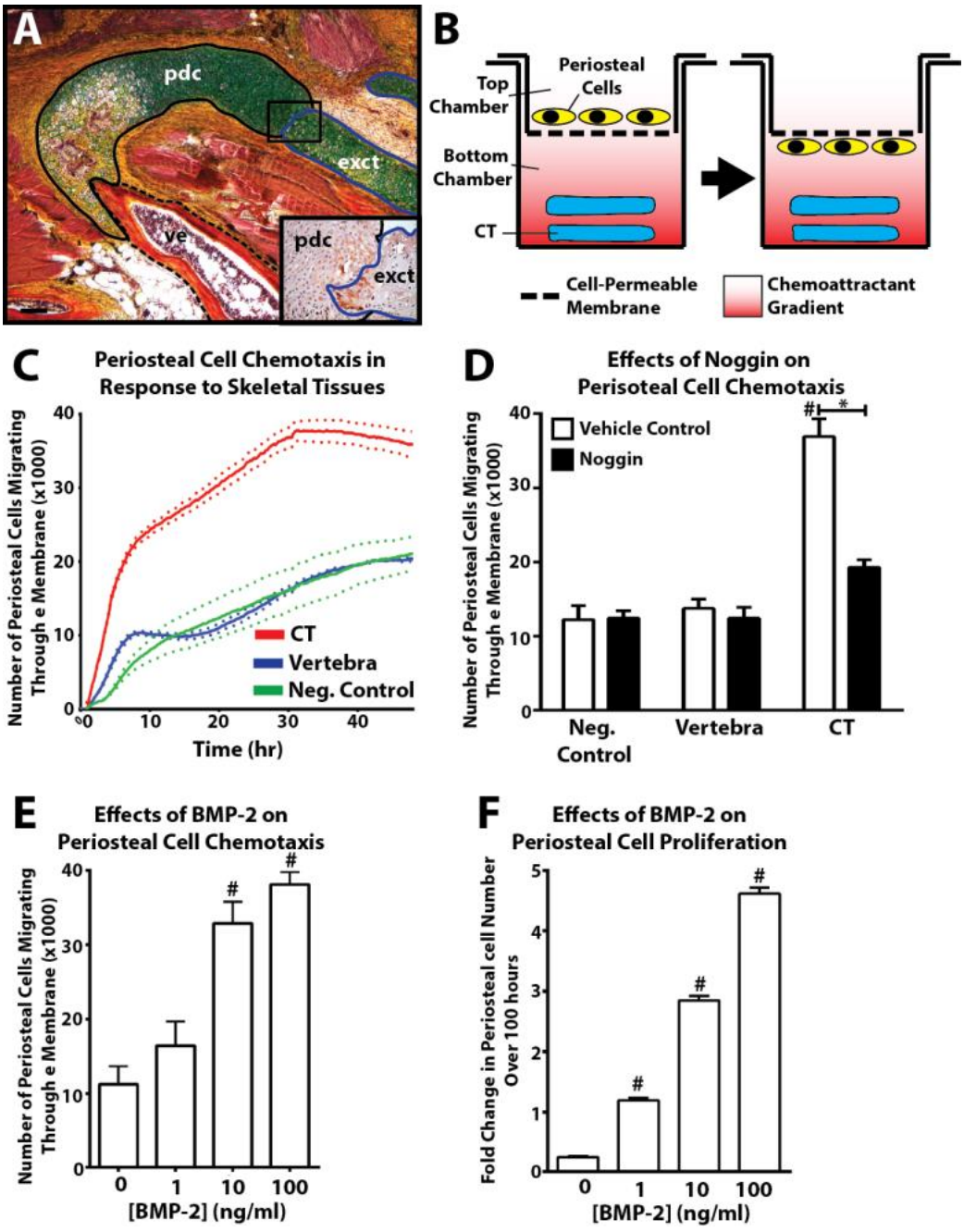

Fig. S21: Lizard CTs induce migration and proliferation in periosteal-derived cells and cartilage via BMP-2. This group of studies considered crosstalk between CC and CT areas and its effect on skeletal regeneration. **(A)** During CT transplantation studies, we observed dramatic expansion and migration/invasion of periosteal-derived cartilage in response to CT implants. Periosteal-derived cartilage was observed bridging gaps between CT implants and vertebrae as they migrated (5/n=5), even creating dramatic bends. Panel A presents histological (pentachrome) analyses of an example of directed CC growth between original tail vertebrae and exogenous CT implants (EXCT), and **(A, Inset)** a higher magnification view of the CC/EXCT interface region immunostained for BMP-2. That CTs were able to induce proliferation and migration of periosteal cell-derived cartilage without direct physical contact suggested that soluble factors secreted by the CTs were involved, and we used migration assays to test the chemotactic effects of CT-derived soluble factors on periosteal cell migration. **(B)** Schematic representing migration assays used to measure effects of lizard

tail tissue on periosteal cell chemotaxis. Migration assays included top and bottom chambers separated by cell-permeable membranes. Chemotaxis was measured as periosteal cell migration from top chambers toward bottom chambers containing CTs. Bottom chambers containing original tail vertebrae were included as tissue-type controls, and empty bottom wells were included as negative controls. In conditions involving lizard CTs and vertebrae, bottom chambers included the same amount of lizard tissues (5 mg wet weight). **(C)** Representative real-time migration assay plot of lizard periosteal cell chemotaxis towards lizard CT or vertebra tissue or vehicle control over 24 hours. Lizard CTs caused significant migration of lizard periosteal cells compared to both negative and tissue-type controls (n=3). These results suggested that factors released by lizard CTs direct migration of periosteal-derived cells.

In order to determine the specific factors responsible for periosteal cell chemotaxis toward CT implants, we screened for signaling molecules expressed at the junction between periosteal-derived cartilage and CT implants. BMP-2 was detected along the interface between the two cartilage regions **(A, Inset)**, similar to the BMP-2 expression pattern observed at the junction between the proximal and CT regions (Fig. S11G). Thus, we hypothesized that BMP-2 was a candidate chemoattractant secreted by the CT that acts on periosteal-derived cartilage. First, the effects of the BMP antagonist noggin on CT-induced periosteal cell chemotaxis was investigated. **(D)** Migration assays were prepared as described above, but with lizard CTs and vertebrae added to bottom chambers in the presence of 100 ng/ml noggin or vehicle control (n=3). Noggin treatment significantly decreased periosteal cell chemotaxis compared to controls, suggesting that BMPs were at least partially responsible for migration induced by CT-secreted factors. **(E)** Finally, we tested the effects of exogenous BMP-2 on periosteal cell migration and proliferation in the absence of CT tissue. Migration assays were prepared with BMP-2 solutions (0-100 ng/ml) in bottom chambers and periosteal cells in top chambers (n=3). BMP-2 proved to be a powerful chemoattractant to periosteal cells, inducing migration in a dose-dependent manner over 24 hours. **(F)** BMP-2 (0-100 ng/ml) also significantly enhanced periosteal cell proliferation in a dose-dependent manner over 100 hours (n=3). Taken together, these results suggest that CT-secreted BMPs, including BMP-2, induce migration and direct expansion of periosteal-derived proximal CCs. This has implications in patterning the proximal regenerated tail CC, and may explain the seamless junction between CC/CT regions with minimal extraneous cartilage development.

Boundaries of original tail vertebra are traced in dashed lines, solid blue lines trace the borders of CT implant, and solid black lines mark the outlines of periosteum-derived cartilage that bridge the gap between vertebrae and CT implants. exct, exogenous cartilage tube implant; pdc, periosteum-derived cartilage; ve, vertebra. Bar = 100 μm. #, $p < 0.05$, compared to vehicle control; *, $p<0.05$, compared to samples indicated by bars.

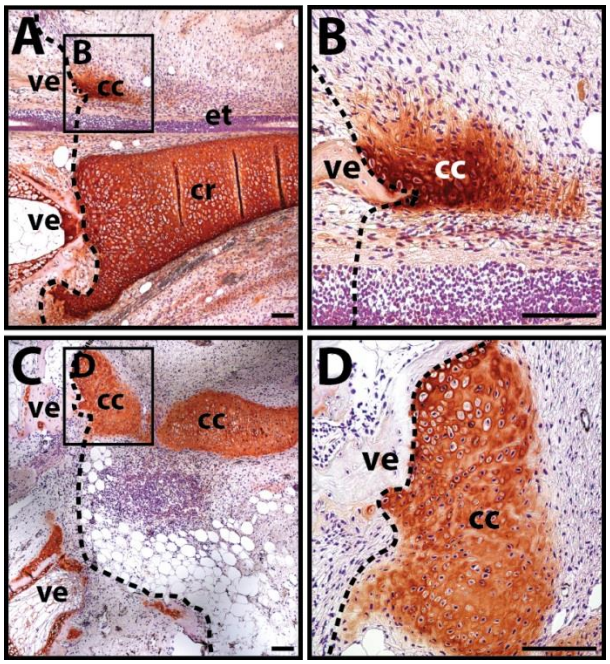

Fig. S22: Salamanders, like lizards, develop vertebra-derived CC regenerated tail regions. Regenerated salamander tails, with or without endogenous spinal cords, were studied for differences in cartilage development. **(A-D)** Sagittal section of proximal regions of regenerated salamander tail analyzed by Col2 immunostaining. **(A)** Control tails with spinal cords developed ventral CRs. Cartilage dorsal to the ependymal tube is only formed at the extreme proximal regenerated tail. **(B)** Magnified view of dorsal cartilage region identified in Panel A highlighting its association with the original tail vertebra. **(C)** Salamander tails without spinal cords did not develop CTs, but extensive cartilage formation was observed in dorsal regenerated tail regions. **(D)** Higher magnification view of dorsal cartilage regions identified in Panel C. Dashed lines denote boundaries between original (left) and regenerated (right) tail regions. cc, cartilage callus; cr, cartilage rod; et, ependymal tube; rsc regenerated spinal cord. Bar = 100 µm.ve, vertebra. Bar = 100 µm.

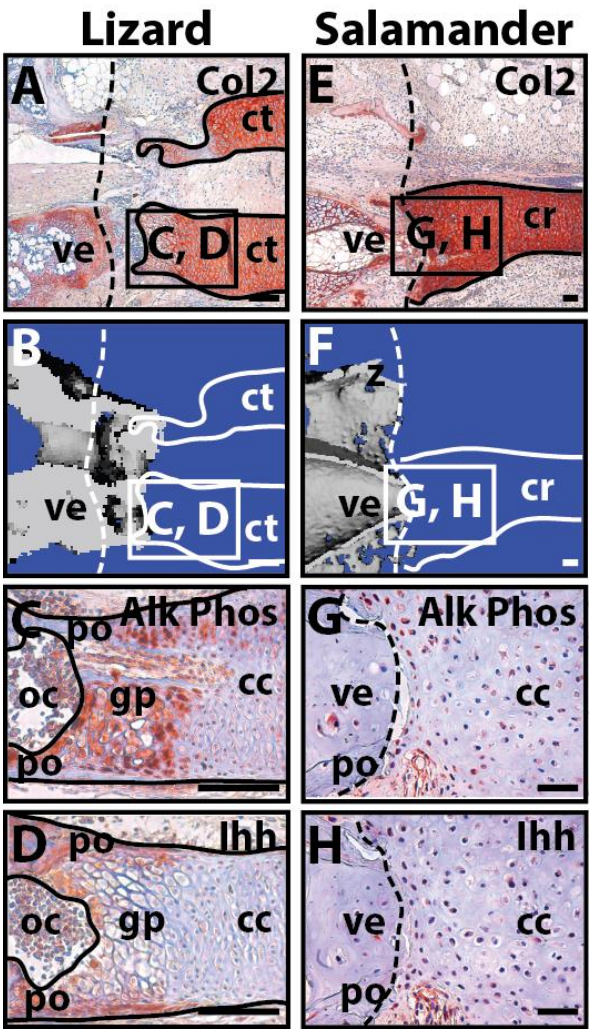

Fig. S23: Proximal lizard, but not salamander, cartilage undergoes endochondral ossification. (A-D) Lizard and (**E-H)** salamander proximal regenerated skeletons (sagittal sections) were analyzed by **(A, E)** Col 2 IHC, **(B, F)** microCT, and **(C, G)** Alk Phos and **(D, H)** Ihh IHC. Dashed lines denote boundaries between original (left) and regenerated (right) tail portions. Solid lines trace outlines of regenerated cartilage skeletons. cc, cartilage callus, cr, cartilage rod; ct, cartilage tube; gp, growth plate-like zone; ip; oc, ossification center; po, periosteum; ve, vertebra. Bar = 100 μm.

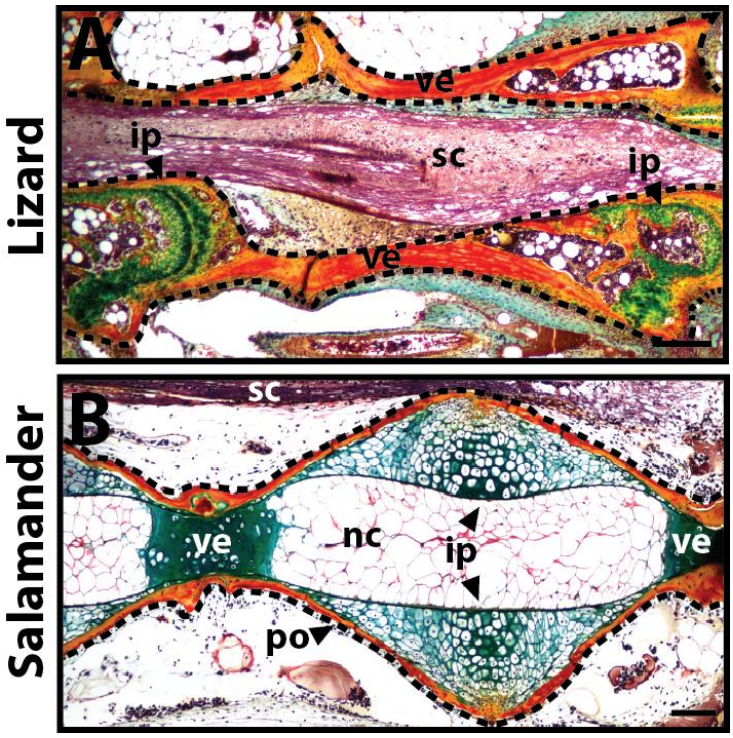

Fig. S24: **Adult lizard tail skeletons are ossified, while adult salamander tail skeletons are predominantly cartilaginous.** Original **(A)** lizard and **(B)** salamander tails analyzed by pentachrome histological staining. Ossified tissue stains red/orange, while cartilage stains green. The majority of lizard tail vertebrae ossify, and cartilage is restricted to unclosed growth plates and intervertebral pads. Salamander tail skeletons retain notochord tissue into adulthood, and the salamander centrum is predominantly cartilaginous (only the periosteum is ossified). Vertebral boundaries are traced in dashed lines. nc, notochord; ip, intervertebral pad; po, periosteum; sc, spinal cord; ve, vertebra. Bar = 100 μm.

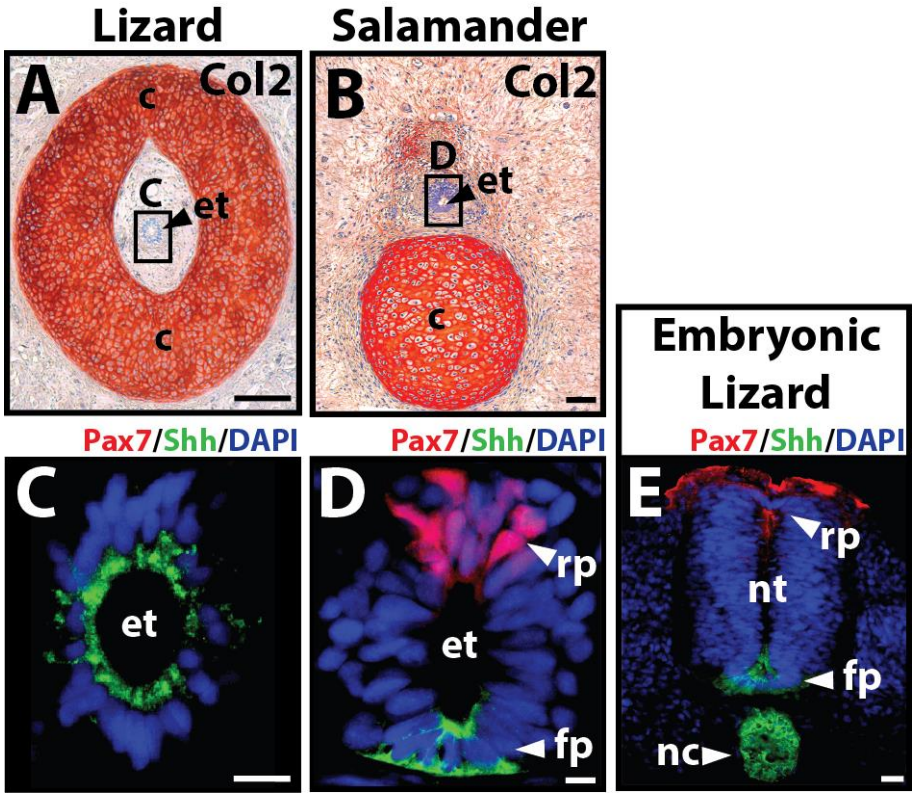

Fig. S25: Salamanders regenerate a cartilage rod, while lizards regenerate a cartilage tube. (A, B) Transverse sections of lizard and salamander regenerated skeletons analyzed by Col2 IHC. Bar = 100 µm. **(C)** Regenerated lizard tail ependymal tube, **(D)** regenerated salamander tail ependymal tube, and embryonic lizard neural tubes analyzed by Shh and BMP-2 IHC. Bar = 25 µm. cr, cartilage rod; ct, cartilage tube; et, ependymal tube; fp, floor plate; nc, notochord; nt, neural tube; rp, roof plate.

Table S1. IHC primary antibody information. Specific primary antibody product information is presented with antigen retrieval methods and antibody dilutions used. Where applicable, comments on antibody performance in IHC applications involving lizard and other animal tissues are also described. For enzymatic antigen retrieval, samples were incubated in 1 mg/ml chondroitinase and 5 mg/ml hyaluronidase for 30 min at 37°C, and for heat-mediated antigen retrieval, samples were treated with sodium citrate buffer, pH 6.0, for 20 min at 95°C followed by 20 min of cooling at room temperature. All primary antibody incubations were performed over 12-16 hours at 4°C. Similarly, all other methodology parameters (i.e., washing, blocking of endogenous peroxidase and nonspecific binding, incubations with secondary antibody and HRP-conjugated streptavidin, signal development, and imaging) were identical among primary antibodies used.

Target	Manufacturer (Product Code)	Antigen Retrieval Method	Antibody Dilution	Comments
Col2	Abcam (ab34712)	Enzymatic	1:400	Excellent reactivity with lizard and salamander tissues.
Shh	Novus Biologicals (NBP1-69270)	Heat-mediated	1:500	Excellent reactivity with lizard and salamander tissues.
Alk Phos	Abcam (ab108337)	Heat-mediated	1:250	Excellent reactivity with lizard and salamander tissues.
Ihh	Abcam (ab39634)	Heat-mediated	1:200	Excellent reactivity with lizard and salamander tissues.
BMP-6	Abcam (ab155963)	Heat-mediated	1:100	Expressed by hypertrophic lizard cartilage.
BMP-2	Abcam (ab14933)	Heat-mediated	1:200	Expressed by junction region at CC/CT interphase.
Col10 [X-AC9]	Abcam (ab140230)	Enzymatic	1:100	Very specific for chick Col10. Does not react with lizard or mammalian samples.
Col10	Abcam (ab58632)	Enzymatic	1:100	Detects Col10 in lizard and chick embryonic growth plate samples.
Pax7	Developmental Studies Hybridoma Bank (PAX7-c)	Heat-mediated	1:50	Excellent reactivity with lizard and salamander tissues.

SUPPLEMENTARY REFERENCES

Colnot, C. (2009). Skeletal Cell Fate Decisions Within Periosteum and Bone Marrow During Bone Regeneration**.** *Journal of Bone and Mineral Research*. **24**, 274-282.

DeLise, A. M., Stringa, E., Woodward, W. A., Mello, M. A., Tuan, R. S. (2000). Embryonic limb mesenchyme micromass culture as an in vitro model for chondrogenesis and cartilage maturation**.** *Methods in molecular biology*. **137**, 359-375.

Limame, R., Wouters, A., Pauwels, B., Fransen, E., Peeters, M., Lardon, F., De Wever, O., Pauwels, P. (2012). Comparative analysis of dynamic cell viability, migration and invasion assessments by novel real-time technology and classic endpoint assays**.** *PloS one*. **7**, e46536.

Lozito, T. P., Tuan, R. S. (2014). Endothelial and cancer cells interact with mesenchymal stem cells via both microparticles and secreted factors**.** *Journal of cellular and molecular medicine*. **18**, 2372-2384.

Mello, M. A., Tuan, R. S. (1999). High density micromass cultures of embryonic limb bud mesenchymal cells: an in vitro model of endochondral skeletal development**.** *In Vitro Cell Dev Biol Anim*. **35**, 262-269.

Sinha, R. K., Morris, F., Shah, S. A., Tuan, R. S. (1994). Surface composition of orthopaedic implant metals regulates cell attachment, spreading, and cytoskeletal organization of primary human osteoblasts in vitro**.** *Clin Orthop Relat Res*. 258-272.